Mon. Not. R. Astron. Soc. **351,** 447–465 (2004) doi:10.1111/j.1365-2966.2004.07509.x

The Canada–UK Deep Submillimetre Survey – VIII. Source identifications in the 3-hour field

Dave Clements,[1,2] Steve Eales,[1⋆] Kris Wojciechowski,[1] Tracy Webb,[3] Simon Lilly,[4] Loretta Dunne,[1] Rob Ivison,[5] Henry McCracken,[6] Min Yun,[7] Ashley James,[1] Mark Brodwin,[8] Olivier Le Fèvre[9] and Walter Gear[1]

[1]*Department of Physics and Astronomy, Cardiff University, PO Box 913, Cardiff CF24 3YB*
[2]*Imperial College, Blackett Laboratory, Prince Consort Road, London SW7 2BZ*
[3]*Sterrewacht Leiden, Postbus 9513, Leiden 2300 RA, the Netherlands*
[4]*Institut für Astronomie, ETH Hönggerberg, HPF G4.1, Zürich CH-8093, Switzerland*
[5]*Astronomy Technology Centre, Royal Observatory, Blackford Hill, Edinburgh EH9 3HJ*
[6]*University of Bologna, Department of Astronomy, via Ranzani 1, Bologna 40127, Italy*
[7]*Department of Physics and Astronomy, University of Massachusetts, 640 Lederle Graduate Research Center, Amherst, MA 01003, USA*
[8]*Department of Astronomy, University of Toronto, 60 St George Street, Toronto, Ontario, Canada M5S 3H8*
[9]*Laboratoire d'Astrophysique de Marseilles, Traverse du Siphon, 13376 Marseille Cedex 12, France*

Accepted 2003 December 3. Received 2003 November 25; in original form 2003 September 12

ABSTRACT

We present optical, near-infrared (IR) and radio observations of the 3-hour field of the Canada–UK Deep Submillimetre Survey (CUDSS). Of the 27 submillimetre sources in the field, nine have secure identifications with either a radio source or a near-IR source. We show that the percentage of sources with secure identifications in the CUDSS is consistent with that found for the bright '8-mJy' submillimetre survey, once allowance is made for the different submillimetre and radio flux limits. Of the 14 secure identifications in the two CUDSS fields, eight are very red objects (VROs) or extremely red objects (EROs), five have colours typical of normal galaxies and one is a radio source that has not yet been detected at optical/near-IR wavelengths. 11 of the identifications have optical/near-IR structures which are either disturbed or have some peculiarity that suggests that the host galaxy is part of an interacting system. One difference between the CUDSS results and the results from the 8-mJy survey is the large number of low-redshift objects in the CUDSS. We give several arguments why these are genuine low-redshift submillimetre sources rather than being gravitational lenses that are gravitationally amplifying a high-z submillimetre source. We construct a K–z diagram for various classes of high-redshift galaxy and show that the SCUBA galaxies are on average less luminous than classical radio galaxies, but are very similar in both their optical/IR luminosities and their colours to the host galaxies of the radio sources detected in μJy radio surveys.

Key words: dust, extinction – galaxies: evolution – galaxies: formation – submillimetre.

1 INTRODUCTION

The luminous high-redshift dust sources discovered by the SCUBA submillimetre and MAMBO millimetre surveys (Smail, Ivison & Blain 1997; Barger et al. 1998; Hughes et al. 1998; Eales et al. 1999; Bertoldi et al. 2000, 2001) are almost certainly of great significance for our understanding of galaxy formation. The ultimate energy source in these objects is hidden by dust but the two obvious possibilities are that (i) the dust is being heated by a hidden active nucleus or (ii) the dust is being heated by a luminous population of stars. The first of these can now largely be ruled out because of the failure of the *XMM–Newton* and *Chandra* telescopes to detect strong X-ray emission from many of the dust sources (e.g. Ivison et al. 2002; Alexander et al. 2003; Almaini et al. 2003; Waskett et al. 2003). Estimates of the star formation rates necessary to produce the dust luminosity can be as high as 6×10^3 $M_\odot$ yr^{-1} (Smail et al. 2003), enough to produce the stellar population of a massive galaxy in $\sim 10^8$–10^9 yr. Many authors have concluded that these dust sources are the ancestors of present-day elliptical galaxies, basing their arguments on estimates of the star formation rate in the population as a whole (Smail et al. 1997; Hughes et al. 1998; Blain et al. 1999), on estimates of the contribution of the sources to the

⋆E-mail: sae@astro.cf.ac.uk

extragalactic background radiation (Eales et al. 1999) and on comparisons of the space-density of the SCUBA/MAMBO sources (henceforth SMSs) with the space-density of ellipticals in the Universe today (Scott et al. 2002; Dunne, Eales & Edmunds 2003).

In view of the probable significance of this population, it is of great importance to determine the optical counterparts to the SMSs and measure their redshifts. If the SMSs are the ancestors of present-day elliptical galaxies, what do the properties of the SMSs tell us about how elliptical galaxies form? There are two rival theories of the birth of an elliptical. In the older of these (Eggen, Lynden-Bell & Sandage 1962; Larson 1975), an elliptical forms when an individual gas cloud in the early Universe collapses, most of the stars of the galaxy forming during the collapse. In the modern theory, the elliptical forms as the result of a sequence of galaxy mergers. This may occur over a relatively long period of cosmic time, with a burst of star formation being triggered during each merger, or it may occur as the result of a few mergers at high redshift (Cole et al. 2000; Percival et al. 2003). If an SMS does represent one of these galaxy-building bursts of star formation, the redshifts of the SMSs are clearly crucial for determining the correct model for elliptical formation. For example, if the older theory is correct, the redshift distribution of the SMSs should probably have a pronounced peak, corresponding to the epoch in which most ellipticals formed.

Unfortunately one of the major problems in understanding this population has been the difficulty of determining the optical counterparts and measuring the redshifts of the SMSs. The obstacles here are the large errors on the positions of the SMSs, which often make it difficult to determine the optical/infrared(IR) counterpart, and the faintness of these counterparts, which make it difficult to measure a redshift. Until recently, the recourse of most groups has been to try to detect the SMSs at radio wavelengths, because the surface density of sources in deep radio surveys is low enough that it is possible to be confident that apparent radio counterparts to SMSs are not chance coincidences. Once an SMS has been securely identified with a radio source, the accurate radio position can be used to determine the optical/IR counterpart. Furthermore, Carilli & Yun (1999) pointed out that, if SMSs are star-forming galaxies like those in the Universe today, it is possible to estimate the redshift of the SMS from the ratio of radio to submillimetre flux. Fortunately, a significant fraction of the SMSs are also faint radio sources. Ivison et al. (2002), for example, found that 60 per cent of the SMSs in the 8-mJy SCUBA survey are also radio sources. The optical objects found at the radio positions are usually faint, often appear to be merging or interacting systems (Lilly et al. 1999; Ivison et al. 2000; Webb et al. 2003c) and often have very red optical–IR ($I - K$) colours, with a significant number being as red as the extremely red objects (EROs) (Ivison et al. 2002; Webb et al. 2003c).

Recently Chapman et al. (2003a) have taken a major step forward by measuring the redshifts for a significant number of SMSs with accurate radio positions. Rather surprisingly, given the dust in these objects, this group succeeded in detecting Lyman α and other UV lines with the Keck telescope from 10 SMSs. The redshifts they have measured lie in the range $0.8 < z < 4$, although because of the requirement for accurate radio positions and because the ratio of radio to submillimetre flux is expected to fall with redshift (Carilli & Yun 1999), this distribution may well be skewed towards low redshifts. Nevertheless, the wide range of redshifts is in better agreement with modern ideas about the formation of ellipticals than with the older theory. The result that a large fraction of SMSs are merging or interacting systems is also in better agreement with these ideas.

In this paper we describe the results of our attempts to determine the optical/IR and radio counterparts to the SMSs in the RA 3^h field of the Canada–UK Deep Submillimetre Survey (CUDSS). Our cosmological assumptions in this paper are $\Omega_\Lambda = 0.7$, $\Omega_M = 0.3$ and a Hubble constant of 75 km s^{-1} Mpc^{-1}.

2 THE SURVEY

The CUDSS (Eales et al. 1999) is one of the largest of the deep SCUBA submillimetre surveys. The basic survey consists of deep 850-μm images of two fields at RA 3^h and 14^h. Each field is approximately 6×8 arcmin^2 in size and the 3σ sensitivity at 850 μm is approximately 3 mJy. This is the eighth paper describing the results from the survey. The first two papers (Eales et al. 1999; Lilly et al. 1999) describe the submillimetre and optical results from initial surveys of parts of the two fields, together with the results from a survey of a third smaller field at RA 10^h. Paper III (Gear et al. 2000) describes millimetre interferometry of the brightest source in the RA 14^h field. Paper IV (Eales et al. 2000) describes the submillimetre observations of the RA 14^h field. Paper V (Webb et al. 2003a) describes an investigation of the cross-clustering between the SCUBA sources and the Lyman break galaxies in the two fields. Paper VI (Webb et al. 2003b, henceforth W2003) describes the submillimetre survey of the RA 3^h field. Paper VII (Webb et al. 2003c) describes the follow-up optical/IR observations of the RA 14^h field. This paper describes the follow-up optical/IR observations of the RA 3^h field. A final paper (Eales et al., in preparation) will describe an investigation of galaxy evolution in the submillimetre waveband using the results from the survey. The 27 sources in the RA 3^h field (W2003) are listed in Table 1.

3 THE OBSERVATIONS

This field was originally observed in the optical and IR wavebands as part of the Canada–France Redshift Survey (Lilly et al. 1995). It has been observed in the mid-IR waveband with the *Infrared Space Observatory* (W2003; Flores et al., in preparation) and in the X-ray waveband with *XMM–Newton* (Waskett et al. 2003). To determine the counterparts to the SCUBA sources, we have used a new radio image obtained with the Very Large Array (VLA), deep IR observations made with the UK Infrared Telescope (UKIRT) and with the Canada–France Hawaii Telescope (CFHT), and optical observations made with the CFHT and the *Hubble Space Telescope* (*HST*).

3.1 Radio observations

We observed this field at 1.4 GHz with the VLA in both the A and B configurations. The reduced radio image and the source catalogue will be presented elsewhere. The noise on the final image was 11 μJy.

3.2 IR observations

We obtained two complementary data sets for the field: observations in the K-band with the IR camera (UFTI) on the UKIRT and observations in the K'-band with the IR camera (CFHTIR) on the CFHT.

3.2.1 UKIRT observations

The UFTI camera on the UKIRT uses a tip–tilt-correcting secondary mirror to deliver images with high angular resolution to an array

Table 1. Submillimetre sources.

(1) Name	(2) RA (J2000)	(3) Dec. (J2000)	(4) S/N	(5) $S_{850\,\mu m}$ (mJy)
CUDSS 3.1	03 02 44.55	00 06 34.5	7.4	10.6 ± 1.4
CUDSS 3.2	03 02 42.80	00 08 1.50	6.7	4.8 ± 0.7
CUDSS 3.3	03 02 31.15	00 08 13.5	6.4	6.7 ± 1.0
CUDSS 3.4	03 02 44.40	00 06 55.0	6.2	8.0 ± 1.3
CUDSS 3.5	03 02 44.40	00 08 11.5	5.8	4.3 ± 0.7
CUDSS 3.6	03 02 36.10	00 08 17.5	5.4	3.4 ± 0.6
CUDSS 3.7	03 02 35.75	00 06 11.0	5.3	8.2 ± 1.5
CUDSS 3.8	03 02 26.55	00 06 19.0	5.0	7.9 ± 1.6
CUDSS 3.9	03 02 28.90	00 10 19.0	4.6	5.4 ± 1.2
CUDSS 3.10	03 02 52.50	00 08 57.5	4.5	4.9 ± 1.1
CUDSS 3.11	03 02 52.90	00 11 22.0	4.0	5.0 ± 1.3
CUDSS 3.12	03 02 38.70	00 10 26.0	4.0	4.8 ± 1.2
CUDSS 3.13	03 02 35.80	00 09 53.5	3.8	4.1 ± 1.1
CUDSS 3.14	03 02 25.78	00 09 7.50	3.5	5.1 ± 1.5
CUDSS 3.15	03 02 27.60	00 06 52.5	3.5	4.4 ± 1.3
CUDSS 3.16	03 02 35.90	00 08 45.0	3.4	2.8 ± 0.8
CUDSS 3.17	03 02 31.65	00 10 30.5	3.4	5.0 ± 1.5
CUDSS 3.18	03 02 33.15	00 10 19.5	3.3	3.9 ± 1.2
CUDSS 3.19	03 02 43.95	00 09 52.0	3.2	3.3 ± 1.0
CUDSS 3.20	03 02 53.30	00 09 40.0	3.2	3.4 ± 1.1
CUDSS 3.21	03 02 25.90	00 08 19.0	3.1	3.8 ± 1.2
CUDSS 3.22	03 02 38.40	00 06 19.5	3.1	3.1 ± 1.0
CUDSS 3.23	03 02 54.00	00 06 15.5	3.1	5.8 ± 1.9
CUDSS 3.24	03 02 56.80	00 08 8.00	3.0	5.1 ± 1.7
CUDSS 3.25	03 02 38.65	00 11 12.0	3.0	4.1 ± 1.4
CUDSS 3.26	03 02 35.10	00 09 12.5	3.0	3.6 ± 1.2
CUDSS 3.27	03 02 28.56	00 06 37.5	3.0	4.0 ± 1.3

(1) Source name. (2) and (3) Position (RA and Dec.) in J2000 coordinates. (4) Signal-to-noise (S/N) ratio with which the submillimetre source was detected (W2003). (5) Flux at 850 μm of source in mJy.

with small pixels (0.0906 arcsec). It can thus provide very deep high-resolution images, which are useful not only for identifying the CUDSS sources but also for providing morphological information, which may help us to understand their origin and nature. The small pixel size of the UFTI, however, has the drawback that many fields would need to be observed to cover completely the region of the submillimetre survey. At present, we have obtained UFTI images of 18 of the 27 sources.

We observed the 3-hour field on the nights of 2000 January 9, 10, 12, 18 and 23 and 2001 October 20–22 in the *K*-band. The camera has a 1024^2 HgCdTe focal-plane array, which gives a field-of-view of 93×93 arcsec^2. Our observations consisted typically of a series of nine short (120 s in the first run, 80 s in the second) integrations, made in a semirandom pattern over a 9×9 arcsec^2 area of sky. After the first group of nine observations, the telescope was offset by 1 arcsec and the same pattern was repeated. Each of these cycles consists of 18 min of integration time (12 min for the later run). We carried out between 6 and 10 of these cycles for each target. To calibrate our observations, we observed stars from the list of UKIRT faint photometric standards several times each night, principally FS7, FS11 and FS30.

We carried out the reduction of the data from each nine-integration cycle using the ORACDR pipeline system, which contains procedures for sky subtraction, flat fielding, the removal of bad pixels and the co-addition and registration of the individual observations. The output of the pipeline is a fully-reduced image of the data from each cycle. For each target, we then aligned and added the images produced by the pipeline, using routines from the Starlink CCDPACK library. The faintest objects visible on the final images have magnitudes between $K \sim 20.5$ and 21.5.

3.2.2 CFHT observations

We observed the 3-hour field in the K' band using the new near-IR camera (CFHTIR) on the CFHT during the period 2001 January 9–15. The seeing was typically 0.8–1.0 arcsec. CFHTIR has 1024×1024 pixels, each with a size of 0.211 arcsec, giving a field-of-view of 3.6×3.6 arcmin^2. We covered two thirds of the area of the 3-hour submillimetre survey with a mosaic of 30-s exposures. We reduced the data using IRAF routines (see Webb et al. 2003c, for more information), producing a single image covering 23 of the 27 CUDSS sources. The total integration time at a typical point in the image is 2.7 h and the faintest detected objects have $K \sim 21.6$.

3.2.3 Deeper images

As a result of these observations, there was often more than one image of a CUDSS source. In order to obtain as deep an image as possible, we co-added the images. We did this using standard procedures within the Starlink library. We first extracted the relevant section of the large CFHT image, binned the UFTI image so that it had pixels of the same size as the CFHT image, aligned the images using objects visible on both images and scaled the images onto a common photometric scale. We then measured the noise on each image and then added the images using as weights the inverse square of the measured noise. We astrometrically calibrated the final images using objects that were visible in both the *K*-band images and in the Canada–France Deep Field (CFDF) *I*-band image (see below). The good agreement between the radio and *K*-band positions (Section 4) implies that in most cases the accuracy of the *K*-band positions is better than 0.5 arcsec.

The final images are shown in Fig. 1. We used the SEXTRACTOR image-detection package to produce catalogues of sources for use in our identification analysis. We obtained *K*-band magnitudes of each potential identification using a circular aperture with a diameter of 3 arcsec.

3.3 Optical observations

The 3-hour field was observed in the optical waveband as part of the CFDF Survey (McCracken et al. 2001). The images obtained as part of this survey consisted of *U*-, *B*-, *V*- and *I*-band images, each covering an area of 0.25 deg^2, and reaching a 3σ limiting AB magnitude of 26.98, 26.38, 26.40 and 25.62, respectively. We used the CFDF images to obtain optical magnitudes for the potential identifications found on the *K*-band image. In all cases, we used the same 3-arcsec aperture as we had used to measure the *K*-band magnitudes. The CFDF *I*-band image of each CUDSS source is shown alongside the *K*-band image in Fig. 1.

For a few of the CUDSS sources there are images taken with the *HST*. Brinchmann et al. (1998) obtained three images with the Wide Field Planetary Camera 2 (WFPC2) in which CUDSS sources fall. These images were taken through the F814W filter and had an integration time of 6700 s. We have also obtained a few WFPC2 images specifically to follow up the CUDSS sources. These images were also taken through the F814W filter and had an integration time of 7000 s. The *HST* data that exist for the CUDSS fields are described in more detail in Webb et al. (2003c).

Note that optical and IR magnitudes given in this paper are based on the Vega zero-points unless otherwise stated.

4 IDENTIFICATION PROCEDURE

The biggest problem in determining the optical counterparts to the SCUBA sources are the large errors in the positions of the sources. The size of the errors is poorly known because of the uncertain effects of nearby faint sources, which are too faint to detected individually, on the positions. Various authors have tried to model this effect (Eales et al. 2000; Hogg 2001; Scott et al. 2002). Eales et al. (2000), for example, carried out an investigation of the positional errors in the CUDSS, using two different methods. They added artificial sources to the real SCUBA images and then compared the positions determined by the source-detection algorithm to the true positions. They also carried out a full-scale Monte Carlo simulation of one of the CUDSS fields and compared the input and output positions of the sources. They concluded that between 10 and 20 per cent of CUDSS sources have measured positions that differ from the true position by >6 arcsec. Scott et al. (2002) have also examined the effect of adding artificial sources onto their real SCUBA maps. They concluded that the mean positional error in their 8-mJy survey is $\simeq$3–4 arcsec. Because the size of the errors is poorly known, it is impossible to use Bayesian statistical techniques (e.g. Sutherland & Saunders 1990). Instead, we and others have adopted the frequentist technique of looking for objects close to the SCUBA position and then estimating the probability of that object being a chance coincidence (e.g. Lilly et al. 1999; Ivison et al. 2002; Serjeant et al. 2003).

The first step in the procedure was to select a radius within which to look for possible counterparts to the SCUBA source. We chose a radius of 8 arcsec, for the practical reason that at larger radii we cannot distinguish a genuine association from a chance coincidence. It is possible, of course, that placing this limit on the search radius will have resulted in our missing some genuine associations. Our investigation of the positional errors in the CUDSS (see above) implies that we will have missed $\simeq$ 5–8 per cent of the associations. However, this estimate is based on simulations. We will show later that we can now empirically estimate the true distribution of positional errors for SCUBA sources (Section 6). This empirical investigation implies that our earlier estimates of the positional errors for SCUBA sources were too pessimistic.

The most useful image for our identification analysis is the radio image because the surface-density of radio sources is sufficiently low, even at the μJy level, that it is possible to determine whether a radio source is genuinely associated with a SCUBA source with high statistical certainty. As the first step in the analysis, we looked for sources within 8 arcsec of the SCUBA position with a peak flux brighter than 40 μJy (3.6σ). There were 11 sources brighter than this limit within 8 arcsec of the 27 CUDSS sources. Any real source should have an angular size at least as large as the angular resolution of the VLA at this frequency (FWHM of 1.4 arcsec) and after analysing the source structures with the AIPS program JMFIT, we eliminated two sources that were probably spurious. The probability of a source detected at >3.6σ within the search area being the result of noise is $\simeq$0.02. Because we have searched around 27 CUDSS sources, the expected number of false radio sources is $\simeq$0.54. Therefore, it is possible that one of the nine radio sources is spurious. However, seven of the nine radio sources are coincident with galaxies (see below) and so are definitely genuine. The exceptions are the sources associated with CUDSS 3.17 and 3.27.

Given that a radio source is genuine, the probability of it not being associated with the SCUBA source is

$$p = 1 - \exp(-d^2 \pi n),$$

in which d is the offset between the SCUBA source and the radio position, and n is the surface density of radio sources. We calculated the surface density of radio sources brighter than 40 μJy using the source counts from the Hubble Deep Field (Richards 2000). The probabilities and offsets are listed in Table 2. Seven of the radio sources have probabilities of being chance coincidences of <1 per cent. The remaining two have probabilities of being chance coinicdences of 3 and 4 per cent. Therefore, all of these radio sources are almost certainly associated with the nine CUDSS sources.

The surface density of objects on the IR images in Fig. 1 is much higher and so we have to use a more sophisticated technique for discriminating between chance coincidences and genuine associations. Because common sense says that a 17th magnitude galaxy 2 arcsec from the SCUBA position is less likely to be a chance coincidence than a 24th magnitude galaxy (because 17th magnitude galaxies are much rarer than 24th magnitude galaxies), we need to find a statistic that incorporates the magnitude of the possible association. We have used the statistic suggested by Downes et al. (1986) to calculate the probability that a candidate galaxy on an IR image within 8 arcsec of the SCUBA position is actually unrelated to the SCUBA source:

$$S = 1 - \exp[-d^2 \pi n(< m)],$$

in which $n(<m)$ is now the surface density of galaxies brighter than the magnitude (m) of the possible association.

The expression above looks like a probability, but it is not because it does not take account of the galaxies on the image that are fainter than the magnitude of the candidate galaxy. If one of these galaxies had been closer to the SCUBA position, it might have had a lower value of S and therefore in deriving the sampling distribution for S this possibility has to be taken into account. Downes et al. (1986) describe an analytic technique for determining the sampling distribution of S. However, because of the effect of clustering and because images do not always have a uniform depth, it is preferable to use a Monte Carlo simulation to determine the probability that a candidate identification that is actually physically unrelated to the SCUBA source has a value of S as low as the measured value. We calculated S for each object within 8 arcsec of the SCUBA position and then used the Monte Carlo technique described by Lilly et al. (1999) to estimate the probability (P) that a physically unrelated object would have such a low value of S. We have listed in Table 2 all the objects that have values for this probability <0.3. As in our earlier paper, we found that the value of P was typically between six and seven times the value of S.

We used the IR images in preference to the optical images for this analysis, because SCUBA galaxies are generally quite red (Smail et al. 2000; Ivison et al. 2002), and so the IR images make it possible to discriminate between genuine associations and coincidences with greater statistical precision than is possible with optical images. There are, however, two SCUBA sources for which there is no object close to the SCUBA position visible on the IR image but for which there is an object visible on the CFDF I-band image. In the case of these two sources, we applied our analysis to the I-band data, although for these sources we calculated P using the analytic relationships in Downes et al. (1986), rather than applying the full Monte Carlo analysis.

Almost all the CUDSS sources for which there are objects on the IR images with values of P less than 0.1 also have radio associations. In most cases, the radio sources coincide, to within the positional

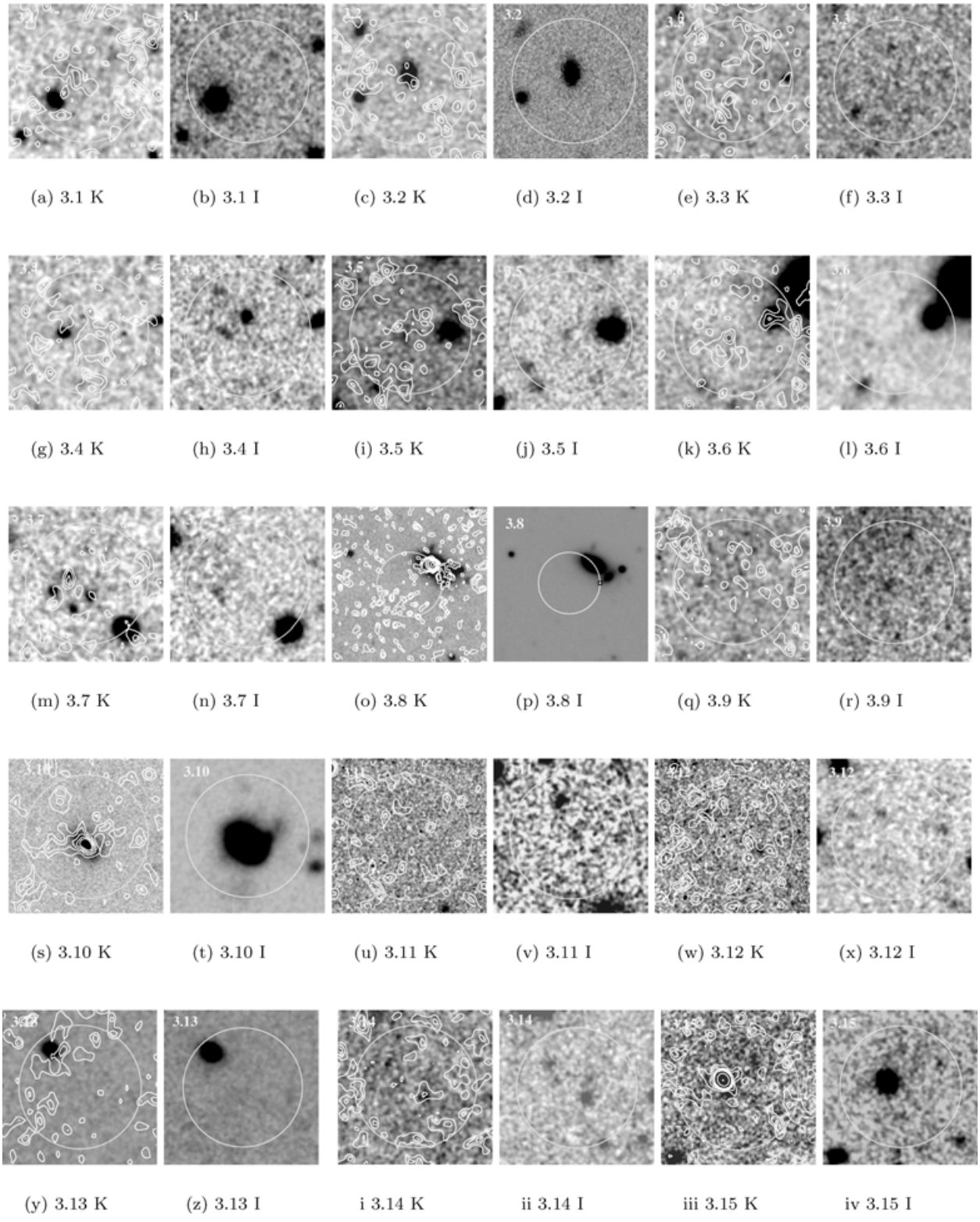

Figure 1. Optical (*I*-band) and near-IR (*K*-band) images of the fields. The *I*-band image is from the CFDF Survey. Each image has a size of 20 × 20 arcsec^2, except for the images of CUDSS 3.8, which have a size of 40 × 40 arcsec^2. The circle on each image is centred on the SCUBA position and has a radius of 8 arcsec. The near-IR image has the radio contours superimposed. The five lowest contours are at intervals of 1σ, 2σ, 3σ, 4σ and 5σ (11, 22, 33, 44 and 55 μJy, respectively), with higher contours being at intervals of 10σ, 20σ, 40σ etc.

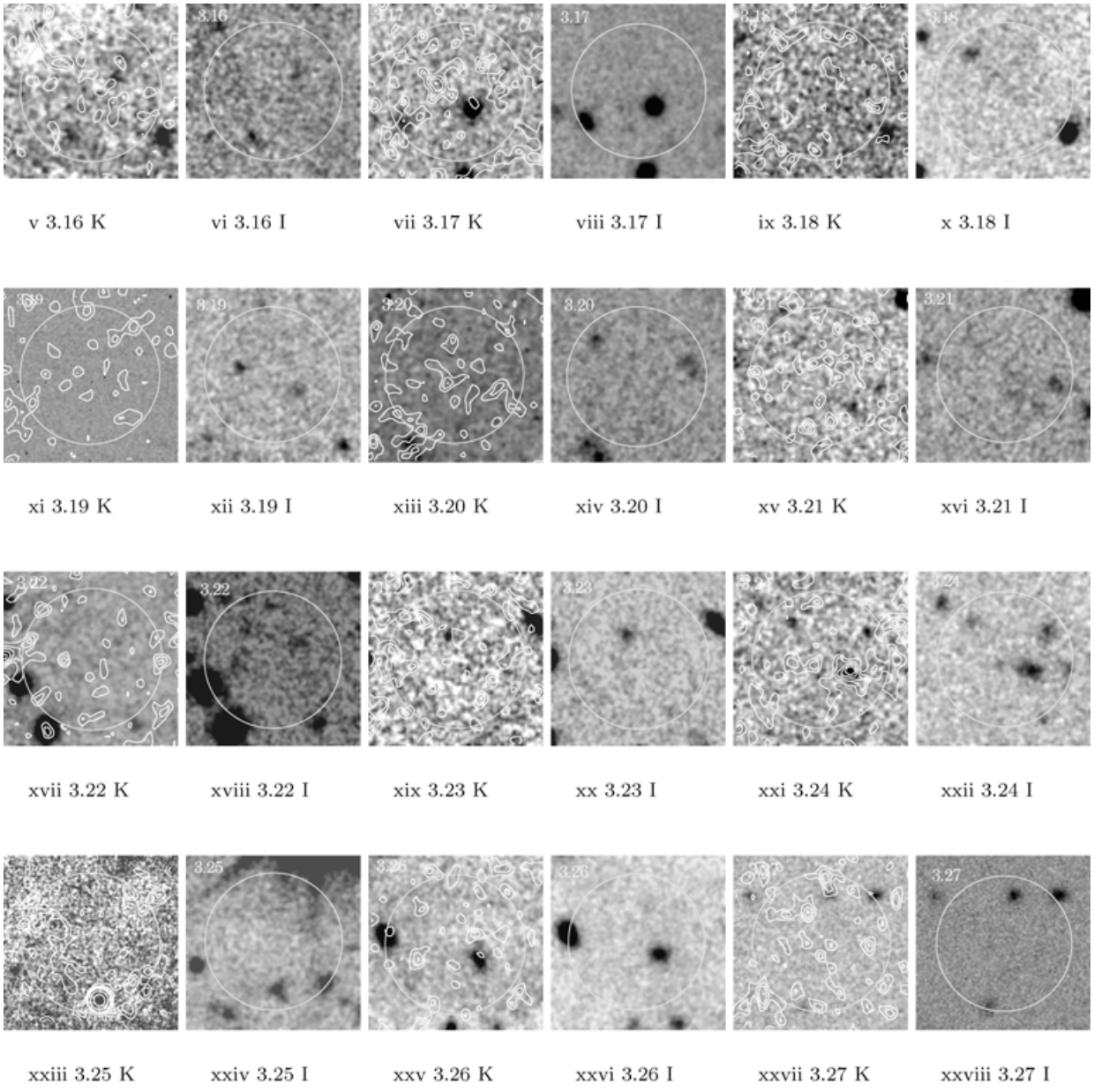

Figure 1 – *continued*

errors, with the IR sources. There are only two CUDSS sources that do not have radio associations but that have possible IR associations. One, CUDSS 3.2, has a value for P of 0.02. The second, CUDSS 3.5, has a value for P of 0.08. If one was considering CUDSS 3.5 in isolation, one would conclude that the galaxy is genuinely associated with the SCUBA source, because the probability of it being a chance projection is only 8 per cent. However, it is not possible to consider the source entirely in isolation. The 3-hour catalogue contains 27 SCUBA sources and, even if there are no galaxies genuinely associated with these SCUBA sources, one expects to find $0.1 \times 27 \simeq 3$ objects on the IR images with values of $P \simeq 0.1$. For this reason, we have decided not to classify this galaxy as a secure identification. In Table 2, we have divided possible identifications into two classes. We have classified all but one of the SCUBA sources with close radio sources, as well as CUDSS 3.2, as having secure identifications. The source we have omitted is CUDSS 3.27, which has two close radio sources. One of these is almost certainly the correct association, but as we are not sure which, we have omitted it from the secure class. We can make a rough estimate of the probability that one of these proposed secure identifications is actually wrong by adding the values of P in Table 2. The total is 0.11, which means the chance of one of these nine secure identifications being wrong is approximately 10 per cent. Our second class of identifications are suspected identifications. We have placed CUDSS 3.5 in this class. Apart from CUDSS 3.27, we have also placed two other SCUBA sources in this class. For these sources, the statistical evidence that the proposed identification is correct is rather weak, but there is circumstantial evidence, based on the similarity of the colour or structure of the galaxy to known SCUBA galaxies, that the identification is correct (see notes on sources).

Table 2. Identifications.

(1) Name	(2) RA (J2000)	(3) Dec. (J2000)	(4) R-(radio), *K*- or *I*-band	(5) Flux or magnitude	(6) Distance from SCUBA position	(7) *P*	(8) Status
CUDSS 3.1	03 02 44.84	00 06 32.0	*K*	19.06 ± 0.02	4.7	0.27	...
CUDSS 3.2	**03 02 42.80**	**00 08 02.5**	***K***	**18.64 ± 0.02**	**1.1**	**0.021**	**Secure**
CUDSS 3.3	.....	.....	..	.....	...	.....	...
CUDSS 3.4	03 02 44.59	00 06 54.9	*K*	19.64 ± 0.03	2.8	0.21	Suspect
CUDSS 3.5	03 02 44.45	00 08 11.1	*K*	21.4 ± 0.2	0.8	0.08	Suspect
CUDSS 3.6	**03 02 36.14**	**00 08 16.8**	**R**	**43 ± 12 μJy**	**1.0**	**0.0006**	**Secure**
	03 02 36.14	**00 08 16.9**	***K***	**21.48 ± 0.21**	**0.9**	**0.066**	...
CUDSS 3.7	**03 02 35.89**	**00 06 11.5**	**R**	**44 ± 12 μJy**	**2.2**	**0.0029**	**Secure**
	03 02 35.90	**00 06 12.0**	***K***	**20.45 ± 0.09**	**2.4**	**0.19**	...
	03 02 35.70	00 06 09.5	*K*	20.54 ± 0.10	1.6	0.11	...
CUDSS 3.8	**03 02 26.15**	**00 06 24.1**	**R**	**683 ± 21 μJy**	**7.8**	**0.038**	**Secure**
	03 02 26.16	**00 06 24.2**	***K***	**14.56 ± 0.003**	**7.8**	**0.074**	...
CUDSS 3.9	03 02 28.95	00 10 18.6	I	24.23 ± 0.05	0.9	0.12	...
CUDSS 3.10	**03 02 52.50**	**00 08 56.4**	**R**	**154 ± 34 μJy**	**1.1**	**0.00076**	**Secure**
	03 02 52.50	**00 08 56.4**	***K***	**16.31 ± 0.005**	**1.1**	**0.0035**	...
CUDSS 3.11	03 02 52.85	00 11 22.1	I	25.0 ± 0.4	0.8	0.15	...
CUDSS 3.12	.....	.....	..	.....	...	.....	...
CUDSS 3.13	03 02 36.06	00 09 58.3	*K*	17.33 ± 0.01	6.1	0.11	...
CUDSS 3.14	03 02 25.68	00 09 06.2	*K*	20.64 ± 0.23	2.0	0.13	Suspect
CUDSS 3.15	**03 02 27.73**	**00 06 53.5**	**R**	**226 ± 12 μJy**	**2.2**	**0.0029**	**Secure**
	03 02 27.72	**00 06 53.2**	***K***	**18.33 ± 0.02**	**2.0**	**0.076**	...
CUDSS 3.16	.....	.....	..	.....	...	.....	...
CUDSS 3.17	**03 02 31.80**	**00 10 31.2**	**R**	**44 ± 12 μJy**	**2.3**	**0.0033**	**Secure**
	03 02 31.52	00 10 28.7	*K*	18.52 ± 0.03	2.7	0.068	...
CUDSS 3.18	.....	.....	..	.....	...	.....	...
CUDSS 3.19	.....	.....	..	.....	...	.....	...
CUDSS 3.20	.....	.....	..	.....	...	.....	...
CUDSS 3.21	.....	.....	..	.....	...	.....	...
CUDSS 3.22	.....	.....	..	.....	...	.....	...
CUDSS 3.23	03 02 54.06	00 06 18.1	*K*	20.75 ± 0.26	2.8	0.20	...
CUDSS 3.24	**03 02 56.58**	**00 08 06.6**	**R**	**122 ± 32 μJy**	**3.6**	**0.0082**	**Secure**
	03 02 56.57	**00 08 06.5**	***K***	**19.26 ± 0.07**	**2.8**	**0.16**	...
CUDSS 3.25	**03 02 38.59**	**00 11 05.3**	**R**	**353 ± 12 μJy**	**6.8**	**0.028**	**Secure**
	03 02 38.58	**00 11 05.5**	***K***	**20.56 ± 0.17**	**6.5**	**0.64**	...
CUDSS 3.26	03 02 34.92	00 09 10.7	*K*	19.58 ± 0.09	3.2	0.14	...
CUDSS 3.27	03 02 28.53	00 06 45.0	R	43 ± 12 μJy	7.5	0.035	...
	03 02 28.67	**00 06 41.2**	**R**	**49 ± 12 μJy**	**3.9**	**0.0097**	**Suspect**
	03 02 28.50	00 06 43.2	*K*	20.27 ± 0.08	5.7	0.62	...

(1) Source name. (2) and (3) Position in J2000 coordinates of the possible counterpart. (4) The waveband in which the possible counterpart was found. An R indicates the counterpart was found on our 1.4-GHz radio image; an *I* or a *K* indicate the standard optical/IR bands. (5) The flux density in μJy of the counterpart if it was found on the radio image; otherwise the *I*- or *K*-band magnitudes of the counterpart. The errors on the *I*- and *K*-band magnitudes do not include the calibration error, which is approximately 0.05 mag. (6) The distance in arcsec between the position of the possible counterpart and the submillimetre position. (7) The probability that the counterpart is not physically associated with the SCUBA source. (8) Our assessment of the proposed identification based on the criteria described in Section 4.

5 NOTES ON INDIVIDUAL SOURCES

5.1 CUDSS 3.1

CUDSS 3.1 is the brightest source in either of the two CUDSS fields. The object listed in Table 1 has a spectroscopic redshift of 0.1952 (Hammer et al. 1995). There is a tentative 450-μm detection (W2003), but the 450-μm position is further from the position of the galaxy than the 850-μm position. Given the large SCUBA positional errors, it is possible that this galaxy is the counterpart to the SCUBA source, but the large value for P means that we have no statistical evidence in favour of this possibility.

5.2 CUDSS 3.2

CUDSS 3.2 is the one source for which there is some circumstantial evidence that gravitational lensing is leading to an incorrect identification. The redshift estimated for the optical counterpart from the broad-band colours (Section 9.2) is 0.62, whereas the estimated lower limit to the redshift of the SMS from the lack of a radio detection (Section 9.1) is 1.7. The large difference in the redshifts suggests that the SMS is behind the galaxy, with the submillimetre flux being gravitationally amplified by the galaxy (Chapman et al. 2002). The undisturbed morphology of the galaxy (Fig. 1) is in agreement with this hypothesis.

5.3 CUDSS 3.4

We have classified the galaxy listed in Table 2 as a suspected identification despite the lack of strong statistical evidence from its position and magnitude, for the following reasons. First, the object has a very red colour ($I - K = 4.14$), which qualifies it as an ERO, and SCUBA sources are frequently found to be associated with EROs (Ivison et al. 2000). Secondly, there is a second much bluer object that is hardly visible on the K-band image but is very prominent on the I-band image (Fig. 1). This is actually closer to the SCUBA position (2 arcsec) and has a slightly lower value of P (0.16, calculated from the statistics of the I-band image). There are some faint signs on the CFDF I-band image (Fig. 1), although not on the *HST* image (Fig. 2), of an interaction between the two galaxies, which is also a common feature of SCUBA galaxies.

5.4 CUDSS 3.5

There are some signs on both the K- and I-band images that this galaxy has a disturbed morphology. This is a common feature of SCUBA galaxies and adds some circumstantial evidence to the statistical evidence that this is the correct identification. We have classed this galaxy as a suspected identification for the reasons described in Section 4.

5.5 CUDSS 3.6

This is a secure identification, because the position of the SCUBA source is only 1.0 arcsec away from a radio source. The faint object visible on the K-band image (Fig. 1) at the radio position has a structure that looks like that of an interacting galaxy.

5.6 CUDSS 3.7

On the K-band image there is a distinctive trapezium of sources. The SCUBA source is detected at radio wavelengths and the radio source is coincident with the northern of the K-band sources. The northern and southern K-band sources are not detected at all in the CFDF I-band image and the limits on their $I - K$ colours (>4.4 and >4.1) place them in the category of EROs. The eastern K-band source is just visible on the I-band image as the northern source of a pair of faint objects. The $I - K$ colour of this source is 3.7, not as red as an ERO but falling within the class of very red objects (VROs) according to the definition of Ivison et al. (2002). The western K-band source is just barely detected in the I-band. The $I - K$ colour is 3.6, making it a VRO. The distinctive arrangement of the sources on the K-band image looks remarkably like a case of gravitational lensing, but the slightly different colours of the sources, and the fact that only one is detected at radio wavelengths, suggests that these sources are not four gravitational images. It therefore seems more likely that the trapezium is actually a cluster of extremely red high-redshift galaxies.

5.7 CUDSS 3.8

Despite the large offset between the radio position and the SCUBA position, there is only a 4 per cent chance that this is a chance coincidence. The peculiar morphology of this galaxy and the fact that it is a strong 15-μm *ISO* source (W2003) are compelling evidence that this is the correct identification (Section 7). The morphology of the system is shown best in the *HST* image (Fig. 2). There are four galaxies and two point sources (presumably stars) visible. Three of the galaxies are spirals. The fourth galaxy has very low surface brightness and is just visible on the western edge of the *HST* image. The *HST* image shows that the two brightest galaxies are interacting. The radio image (Fig. 1) shows that both of these galaxies are also radio sources. The radio emission is probably the result of starbursts triggered in both galaxies by the interaction. The brightest galaxy has a spectroscopic redshift of 0.088.

5.8 CUDSS 3.9

There is nothing visible on the K-band image (Fig. 1). There is, however, a faint galaxy visible both on the I-band image from the CFDF survey and on the *HST* image (Fig. 2). The value of P given in Table 2 has been calculated from the statistics of the CFDF I-band image.

5.9 CUDSS 3.10

CUDSS 3.10 has a secure identification, with the radio position only 1.1 arcsec away from the SCUBA position. We showed in our previous paper (W2003) that this SCUBA source is also identified with an *ISO* 15-μm source, the *ISO* position also being only 1.5 arcsec from the SCUBA position. There is a bright galaxy coincident with the radio position with a spectroscopic redshift of 0.176 (Hammer et al. 1995). The I-band CFDF image (Fig. 1) and especially the *HST* image (Fig. 2) suggest that the galaxy is involved in a merger.

5.10 CUDSS 3.11

There is a very faint object visible on the CFDF I-band image (Fig. 1). It is only 0.75 arcsec from the SCUBA position. However, because of the high surface density of objects at this faint magnitude, the probability that it is physically unrelated to the SCUBA source is 15 per cent.

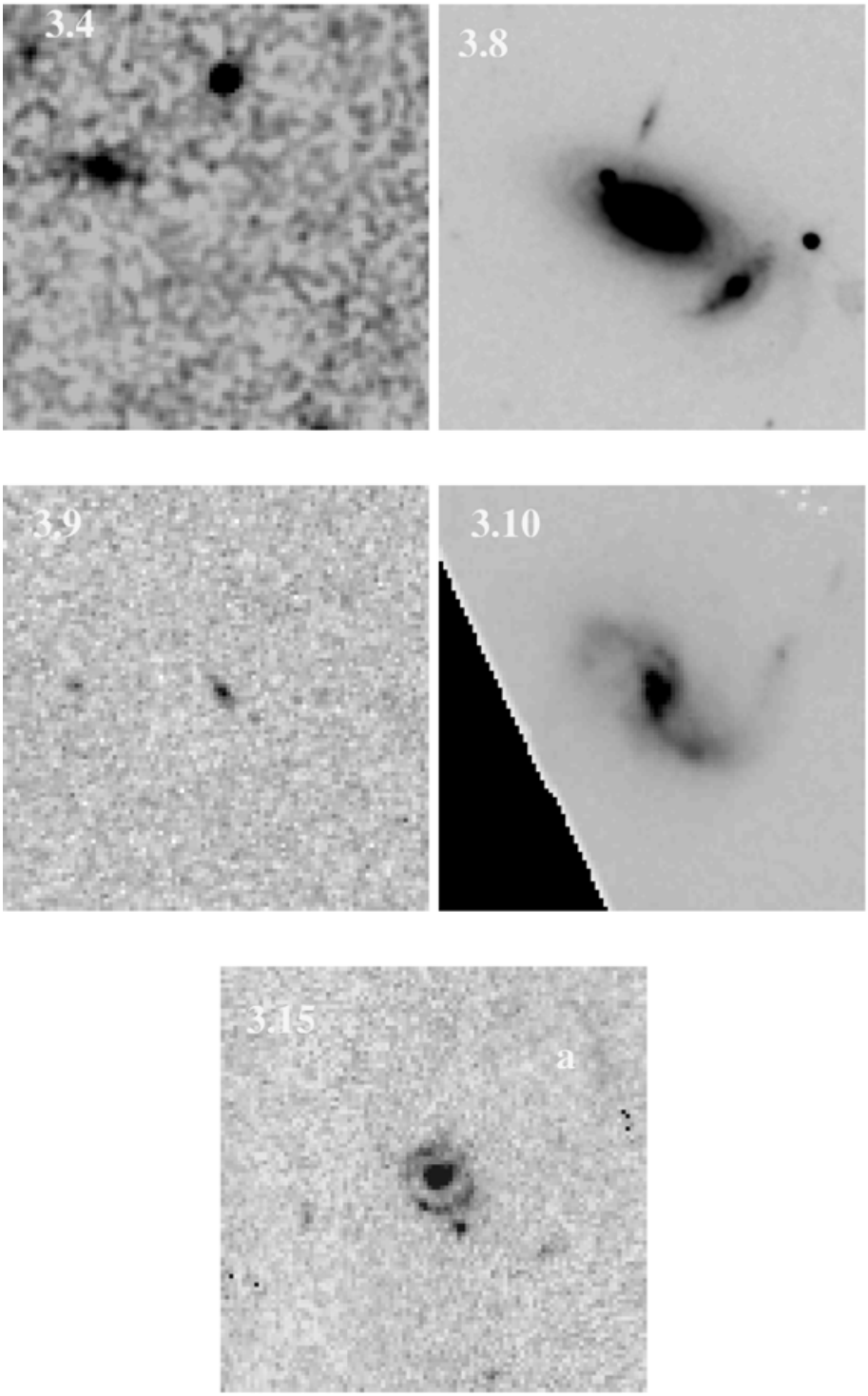

Figure 2. *HST I*-band images of five of the fields. Each image has a size of 5 × 5 arcsec^2, except for the image of CUDSS 3.8, which has a size of 10 × 10 arcsec^2.

5.11 CUDSS 3.14

The probability that the object listed in Table 2, which is 2 arcsec from the SCUBA position, is physically unrelated to the SCUBA source is 13 per cent and therefore above our threshold for a secure identification. We have, however, listed it as a suspected identification because of the other faint objects visible in the CFDF *I*-band image, some of which are even closer to the SCUBA position. The objects look remarkably like a high-redshift cluster, with the object listed in Table 2 being the brightest galaxy in the cluster. This is circumstantial evidence in favour of our proposed identification because, as we will show later in this paper (Section 10), SCUBA galaxies can have optical/near-IR luminosities as high as radio galaxies or first-ranked cluster galaxies.

5.12 CUDSS 3.15

CUDSS 3.15 has a secure identification, with a radio source lying only 2 arcsec from the SCUBA position. The source was also detected with *ISO* at 15 μm (W2003). On the *K*-band and CFDF *I*-band images (Fig. 1) the galaxy looks unexceptional, but the *HST* image (Fig. 2) shows a ring at the centre of the galaxy, approximately 1 arcsec across, encircling a point source. There is also a faint arc on the *HST* image (labelled 'a' in Fig. 2). We cannot decide between two possible interpretations of this system. One possibility is that the object is an example of a collisional ring galaxy. These objects are thought to be the result of the head-on collision between two galaxies, one of which has travelled along the spin-axis of the other, striking the disc of the second galaxy close to its centre (Appleton & Marston 1997). From the multiband optical and IR photometry of the identification we estimate that its redshift is $\simeq$0.7 (Section 9.2). At this redshift, the physical size of the ring would be typical of those seen in ring galaxies (Appleton & Marston 1997). In this interpretation, the arc seen on the *HST* image would represent tidal debris from the collision. The alternative interpretation is that the ring and arc represent a gravitational-lensing phenomenon. The size of the ring is approximately what one expects for an Einstein ring produced by a lens with the mass of a typical galaxy. In view of the 15-μm emission from this galaxy (Section 7), we suspect the former explanation is the correct one.

5.13 CUDSS 3.17

CUDSS 3.17 has a secure identification, with the radio source only 2.3 arcsec from the radio position. However, there is nothing visible on either the *I*-band or *K*-band image at the position of the radio source.

5.14 CUDSS 3.22

In W2003 we argued that the CUDSS 3.22 SCUBA source is identified with a 15-μm *ISO* source. The *ISO* position is 7.5 arcsec from the SCUBA position and so is indeed within our search radius. However, the two galaxies that are the possible counterparts to the *ISO* source are both outside the search radius. Indeed, it now seems likely that it is the galaxy that is the furthest from the SCUBA position that is the true counterpart to the *ISO* source, because this galaxy is also a radio source. We therefore no longer think it is likely that the *ISO* and SCUBA sources are related. There are a number of possible identifications visible on the CFDF *I*-band image, but none with a very low value of *P*.

5.15 CUDSS 3.24

CUDSS 3.24 has a secure identification, with a radio source only 3.6 arcsec from the SCUBA position. The galaxy visible at the radio position (Fig. 1) is also a 15-μm *ISO* source (W2003). The $I - K$ colour of the galaxy is 3.50, which puts it in the category of VROs (Ivison et al. 2002).

5.16 CUDSS 3.25

CUDSS 3.25 has a secure identification. The radio source is 6.8 arcsec from the SCUBA position but the probability that this is a chance coincidence is only 3 per cent. The CFDF *I*-band image shows something that looks like two interacting galaxies, which is circumstantial evidence that the identification is correct.

5.17 CUDSS 3.26

The probability of the galaxy being unrelated to the SCUBA source is 14 per cent and thus the statistical evidence that this is the correct identification is weak. A piece of circumstantial evidence that this is the correct identification is the different morphologies visible on the *I*- and *K*-band images. The structure on the *K*-band image extends to the south, suggesting that there may be two objects, a normal galaxy and a very red object, which only becomes visible on the *K*-band image. This is a situation that has been seen for other SCUBA sources (Smail et al. 2002; Chapman et al. 2002).

5.18 CUDSS 3.27

This is a rather peculiar field because there are two radio sources, both of which have low values of *P*, and it is not clear which is the correct identification. We have selected the radio source that is closest to the SCUBA position (and thus has the lowest value of *P*) as the probable identification. Nevertheless, there are strong circumstantial arguments for the other source being the correct identification because it is both a 15-μm *ISO* source (W2003) and the galaxy associated with the source has a disturbed morphology (see the *K*-band image in Fig. 1). The second radio source is, however, much closer to the SCUBA position. There is nothing on either the *K*- or *I*-band image at the position of this radio source.

6 RELIABILITY OF SURVEY

All of the teams carrying out SCUBA surveys have recognized that some of their sources are likely to be spurious, because many of the sources are detected with low signal-to-noise ratios and the surveys are often close to the confusion limit. In earlier papers (Eales et al. 2000, W2003) we estimated that 10 per cent of the CUDSS sources are likely to be spurious, based on both Gaussian statistics and on the results of applying our source-detection algorithm to negative maps. Because any SCUBA source with a secure identification is likely to be a genuine submillimetre source, we can use the results of the previous sections to investigate empirically the reliability of the CUDSS survey. In this section we also compare the results of our identification analysis with the results of a similar analysis for the 8-mJy SCUBA survey, the other large-area blank-field SCUBA survey.

The 8-mJy survey contains 36 sources detected at $>3.5\sigma$ with 850 μm flux densities $\geqslant$8 mJy in an area of sky of 260 arcmin^2 (Scott et al. 2002). Thus the survey is less sensitive but covers a larger area than CUDSS. The expected percentage of spurious sources, based on Gaussian statistics, is approximately half the value expected for CUDSS. Ivison et al. (2002) have shown that the fraction of 8-mJy sources with radio associations drops systematically in areas of the original submillimetre images with high noise. They have used this fact to argue that six of the 8-mJy sources are likely to be spurious. After removing these six sources from the catalogue, they find that 60 per cent of the 30 remaining 8-mJy sources are detected at radio wavelengths.

The first thing we can do is compare the percentages of SCUBA sources with radio associations in the two surveys. Nine out of 27 sources in the CUDSS 3-hour field and five out of 23 sources in the CUDSS RA 14-hour field (Eales et al. 2000; Webb et al. 2003c) have radio detections. These are much lower percentages than are found for the 8-mJy survey. However, the difference can almost certainly be attributed to the different sensitivities, at both submillimetre and radio frequencies, of the different surveys. To

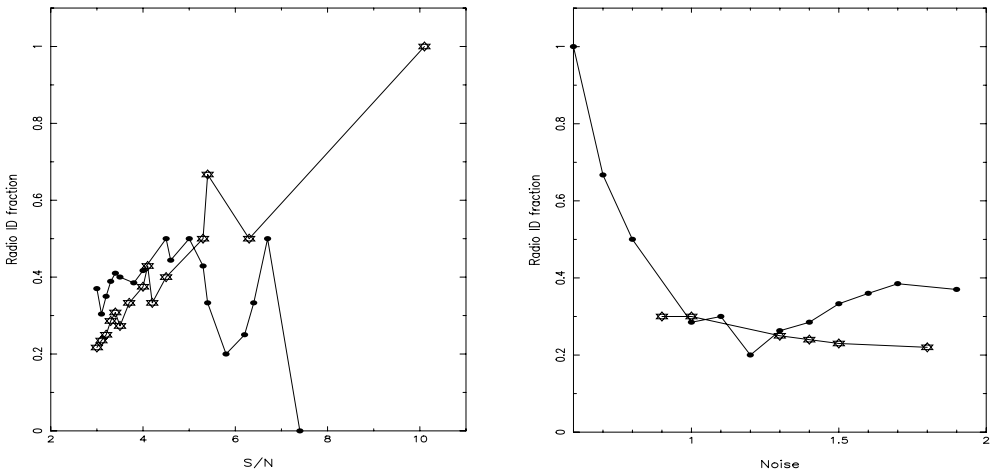

Figure 3. Plots of cumulative fraction of SCUBA sources with radio detections against the signal-to-noise ratio with which a source was detected in the original SCUBA survey (left-hand plot) and against the noise in the original SCUBA survey at the position of the source (right-hand plot). The stars represent the results for the 14-hour field, the circles the results for the 3-hour field.

show this, we have compared the radio and submillimetre surveys of the CUDSS 3-hour field with the corresponding 8-mJy surveys. We have excluded the CUDSS RA 14-hour field because the radio observations were made at 5 GHz, which makes the comparison difficult. Let us assume that the redshift distributions of the objects in the CUDSS and 8-mJy survey are similar. The 8-mJy sources are, on average, a factor of $\sim$2 brighter than the CUDSS sources at 850 μm. If the redshift distributions are the same, they will also be brighter by a similar factor at 1.4 GHz. To investigate the effects of the flux limits, we have decreased the radio flux of each 8-mJy source (Ivison et al. 2002) by this factor. This decrease now makes the 8-mJy sources directly comparable to the CUDSS sources. Only seven of the 8-mJy sources now have radio fluxes that fall above the 40 μJy limit of our radio observations. Thus the higher percentage of radio detections for the 8-mJy survey is entirely the result of the different flux limits of the two surveys.

We have followed Ivison et al. (2002) in using the statistics of the radio detections to investigate the reliability of the CUDSS survey. Fig. 3 shows the fraction of SCUBA sources that are also radio sources as a function of both the signal-to-noise ratio in the original submillimetre survey and of the noise at the position of the source in the original submillimetre image. Because of the small number of sources, we have expressed this as a cumulative fraction. In the 3-hour field, the fraction of radio detections clearly does not depend on the signal-to-noise ratio. In this field the radio fraction does appear to increase at low values of the submillimetre noise, but because this increase is the result of only four out of the 27 sources (of which two are radio detections), we do not regard it as significant. In the 14-hour field, the radio fraction does appear to depend on the signal-to-noise ratio but does not depend on the value of the submillimetre noise. Ivison et al. (2002) used the result that the radio fraction falls with increasing submillimetre noise in both of the 8-mJy fields to eliminate sources in regions of high noise. Because there is no similar effect that occurs in both of the CUDSS fields, we conclude there is no compelling statistical evidence to eliminate CUDSS sources below some signal-to-noise ratio threshold or in regions of high noise.

A final useful thing we can do with the identification statistics is to derive empirically the distribution of SCUBA position errors. In an earlier paper (Eales et al. 2000), we used a Monte Carlo simulation to predict the distribution of position errors, but it is preferable to determine these directly. Because the radio positions have an accuracy of better than 1 arcsec, the offset between the radio position and the submillimetre position of a source is a direct measurement of the error in the submillimetre position. There is one caveat to this. If there are errors greater than 8 arcsec, we will miss them, because that was the maximum distance out to which we looked for radio sources (Section 4). Fig. 4(a) shows the histogram of positional errors for the 14 CUDSS sources with radio detections, overlaid with the distribution of errors predicted from our Monte Carlo simulation (Eales et al. 2000). Fig. 4(a) shows that in practice our positions are slightly more accurate than the Monte Carlo simulation predicted. For example, 3 out of 14 sources (21 per cent) have positional errors $\leqslant$1 arcsec, whereas our simulation predicted that there would be essentially no sources with position errors this small.

Fig. 4(b) shows the positional errors derived in the same way for the 8-mJy sample (Ivison et al. 2002). In the case of the 8-mJy sources, we may be slightly biased towards small positional errors, because the deeper radio data means that a source $>$4 arcsec from the submillimetre position can not always be confidently associated with the submillimetre source (Ivison et al. 2002). Because the 8-mJy survey is further from the submillimetre confusion limit than the CUDSS, one might expect the accuracy of the positions to be rather better. However, the CUDSS positions are at least as good. For example, five out of 14 CUDSS sources have positional errors $\leqslant$2 arcsec compared with four out of 18 8-mJy sources. This comparison lends some support to the elaborate, if not very elegant, cleaning technique we used to produce the source catalogue (Eales et al. (2000); W2003).

7 THE IDENTIFICATIONS AT LOW REDSHIFT – GRAVITATIONAL LENSING?

Our identification analysis is based entirely on calculating the probability that an object, either a radio source or a faint galaxy, would fall so close to the position of a SCUBA source by chance. There is one possible weakness in this approach. If a significant fraction of the SCUBA sources are gravitationally lensed, then it is possible that this technique will find the lens rather than the galaxy that is genuinely responsible for the submillimetre emission. Because the lens will always be at a lower redshift, this method could produce

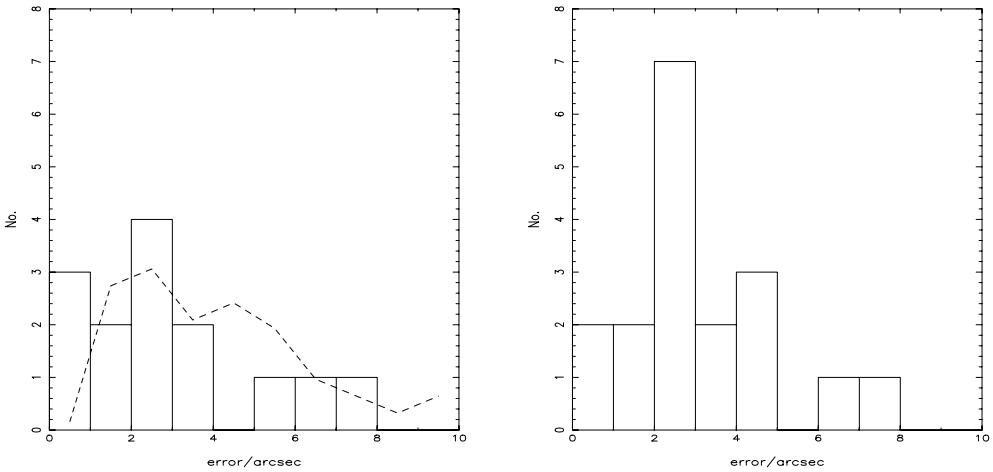

Figure 4. Offsets between the radio and submillimetre positions for submillimetre sources that have radio detections. Because the radio positions are very accurate, these offsets are effectively the errors on the submillimetre positions. The left-hand figure is for the CUDSS. The dashed line shows the prediction we made for the CUDSS positional errors from a Monte Carlo simulation (Eales et al. 2000). The right-hand figure shows the same histogram for the 8-mJy sample, using the data in Ivison et al. (2002).

spurious low-redshift identifications for SCUBA sources (Chapman et al. 2002).

The CUDSS contains a larger number of low-redshift identifications than were found in the 8-mJy survey (Ivison et al. 2002). Our small pilot survey at RA $10^{\rm h}$ contained two sources that have identifications with spectroscopic redshifts <1 ($z = 0.074$ and 0.55, Lilly et al. 1999). The two large fields contain three sources with identifications with spectroscopic redshifts below this limit ($z =$ 0.088, 0.176 and 0.66) plus two sources with identifications with estimated redshifts (from the broad-band colours, Section 9.2) below this limit. Might some of these objects actually be a lens rather than the galaxy responsible for the submillimetre emission?

There are three arguments that this is not generally the case. The first of these is described in detail in Section 9, in which we show that the redshift estimated for the galaxy from multiband photometry is generally very similar to the redshift estimated for the SMS from the ratio of radio-to-submillimetre flux. The second argument is based on the morphologies of the galaxies. If the galaxies are lenses, they should be galaxies that just happen to fall between the SCUBA source and the Earth, with the only bias in their properties being that they will tend to be galaxies that produce large gravitational amplification factors. There is no reason to expect them to have the morphological peculiarities characteristic of SCUBA galaxies. However, many of our low-redshift galaxies are indeed extremely peculiar systems. Good examples are the systems of interacting galaxies CUDSS 3.8 and 3.10 (Fig. 2).

The third argument is based on the fact that most of the low-redshift identifications are also *ISO* 15-μm sources. We have 15-μm observations of the 3-hour and 14-hour fields but not of the 10-hour field. Of the five low-redshift objects in the former fields, four are detected at 15-μm (note that we did not use the 15-μm results in our identification analysis, Section 4). The typical shape of the spectral energy distribution of galaxies means that galaxies are unlikely to be detected at 15 μm at $z \geqslant 1$ (Eales et al. 2000; Flores et al. 1999). It is therefore unlikely that a SCUBA source at $z \gg 1$ that is being lensed by a low-redshift galaxy will be detected at 15 μm. It is possible that the SMS is being lensed but the 15-μm emission is from the lens rather than the SMS. By comparing the surface density of 15-μm sources with the surface density of galaxies with $K < 20$ (Cowie et al. 1994; Flores et al. 1999), we estimate that the probability of a lens also being a 15-μm source is roughly 10 per cent. Therefore, the probability that four out of five lenses are also 15-μm sources is clearly extremely low.

One source, CUDSS 3.2, may be the exception that proves the rule. It is the one low-redshift SMS that is not detected at 15 μm; the optical counterpart has an undisturbed morphology; and the redshift estimated for the counterpart from multiband photometry (0.62, Section 9.2) is much lower than the redshift limit estimated from the ratio of radio-to-submillimetre flux (>1.7, Section 9.1). These properties are all consistent with the hypothesis that the optical counterpart is actually a lens that is gravitationally amplifying the radio and submillimetre emission from an SMS at a much higher redshift. However, the difference in all three respects between this object and the other low-redshift counterparts strongly suggests that the latter SMSs are genuinely at low redshift.

Of the 50 SMSs in the two large fields, there is only 1 source for which there is plausible evidence for lensing. Blain (1998) predicted that approximately 2 per cent of SMSs with $S_{850\,\mu{\rm m}} \simeq 10$ mJy are gravitationally amplified by a factor of $\geqslant 2$. This is the same as our observed fraction, although the prediction is for a different flux level.

We cannot not use the arguments above for the two sources in the 10-hour field because we have no 15-μm data for this field. However, both these sources are also detected at 450 μm. Because the ratio of 450- and 850-μm fluxes is expected to fall with redshift (fig. 8 of Eales et al. 2000), the detection of these sources at 450 μm is strong circumstantial evidence that the low-redshift identifications are correct.

If the gravitational-lensing hypothesis can be eliminated, is there any other effect that might produce spurious low-redshift identifications? There is one effect that might be important. At the submillimetre flux level of the CUDSS, the confusion of faint sources is likely to be important. Our Monte Carlo simulations (Eales et al. 2000) revealed the possible importance of flux-boosting, in which an apparent single source is actually two or more sources, which are only in the survey because their combined fluxes are greater than the flux limit of the survey. If this is the case for any of our sources, then it is possible that there are two or more genuine identifications close to the submillimetre position, but we have only found

the identification at the lower redshift. There is one possible example of this. CUDSS 3.27 has two possible counterparts, each with a low value of P (Section 5). In this case, we rejected the counterpart that is detected at 15 μm because it has a higher value of P than the alternative. However, it is possible that both identifications are correct.

Finally, we note that although the fraction of sources with low-redshift identifications is higher in the CUDSS than in the 8-mJy survey, the estimated redshifts of the sources in the 8-mJy survey with submillimetre fluxes below 8 mJy are, on average, 0.6 lower than the estimated redshifts of the sources above this flux limit (Ivison et al. 2002). This is additional evidence that the phenomenon that the fraction of sources with low redshifts is increasing as the submillimetre flux limit decreases is a genuine one.

8 THE NATURE OF THE IDENTIFICATIONS – MORPHOLOGIES AND COLOURS

There are 14 secure identifications in the 3-hour and 14-hour fields (this paper and Webb et al. 2003c). Of these, one is not detected at IR or optical wavelengths and so it is impossible to classify the morphology of the galaxy; two show no signs of an interaction or have no morphological peculiarity; the remaining 11 show some signs of an interaction or have some peculiarity in the structure. Ivison et al. (2002) performed a similar analysis for the 8-mJy sample. Of the 21 secure identifications, they listed six as being too faint at optical/IR wavelengths to classify morphologically; 13 as being distorted or close multiple systems; and two as being compact. Given the subjectivity in making classifications of this kind, the proportions seem quite similar in the two surveys.

We are on stronger ground in classifying galaxies according to their colours. Ivison et al. (2002) divided galaxies into EROs ($I - K > 4$) and VROs ($3.3 < I - K < 4.0$). Of 18 SCUBA sources with radio detections, they found that seven objects had normal colours, 10 objects could be classified as either a VRO or an ERO and one source was not detected at optical/IR wavelengths. Of our 14 secure identifications, we find five objects with normal colours, eight objects that are either VROs or EROs and one object that is not detected at IR or optical wavelengths. The proportions of objects in the different classes are thus remarkably similar for the two samples.

9 ESTIMATING REDSHIFTS

Chapman et al. (2003a) have recently succeeded in using the Keck telescope to measure redshifts for 10 SCUBA sources, the first significant number of SCUBA galaxies for which this has been done. However, despite this important success, it is likely that methods for estimating redshifts will be important for several years to come. First, Chapman et al. (2003a) only targeted SCUBA sources that were detected at radio wavelengths and had I magnitudes $22.2 < I < 26.4$, and thus their results are strictly applicable only to the ∼50 per cent of the SCUBA population that satisfy these limits. Because the ratio of radio-to-submillimetre flux is expected to fall with redshift (Carilli & Yun 1999), the radio criterion, in particular, is likely to lead to an underestimate of the proportion of SCUBA sources with $z \geqslant 2$. Secondly, Chapman et al. (2003a) only succeeded in measuring redshifts for approximately 30 per cent of the sources that satisfied the above criteria. The sources for which they failed may either have weak emission lines or be at a redshift at which emission lines are hard to detect (Chapman et al. 2003a noted the relative lack of SCUBA galaxies in the redshift range $1 < z < 2$, the so-called redshift desert, a redshift interval in which few strong emission lines fall in the optical waveband). For these reasons, methods for estimating redshifts of SCUBA galaxies are likely to continue to be important.

In this section, we investigate two methods for estimating redshifts. Both are well known but only one has been applied before to SCUBA galaxies. In both cases, we have used the spectroscopic redshifts that do exist for SCUBA galaxies, both from the work of Chapman et al. (2003a) and from our own work, to test the efficiency of the methods.

9.1 The radio method

Carilli & Yun (1999) were the first to point out that for a star-forming galaxy the ratio of radio-to-submillimetre flux should be a function of redshift and thus that it should be possible to estimate the redshift of a star-forming galaxy from this ratio. Following the original suggestion, a number of groups used different samples of low-redshift objects to determine the expected relationship between this ratio and redshift (Carilli & Yun 2000; Dunne, Clements & Eales 2000b; Rengarajan & Takeuchi 2001). There are slight differences between the redshifts estimated using the different sets of low-redshift templates (Ivison et al. 2002).

Fig. 5 shows the ratio of submillimetre-to-radio flux plotted against redshift for all SCUBA galaxies that have both spectroscopic redshifts and radio measurements. We have plotted on the figure the predictions for star-forming galaxies using the 104 low-redshift templates of Dunne et al. (2000b). As described in that paper, we first predict the relationship between the flux ratio and redshift for each template and then, at each redshift, determine the median and $\pm 1\sigma$ predicted values of the flux values. The one slight difference from that paper is that the templates have been modified to incorporate our 450-μm observations of the galaxies (Dunne & Eales 2001).

At first sight, the diagram does not instill one with much confidence in the method, because for the high-redshift data there is not even a strong correlation between the the flux ratio and redshift. The diagram also suggests that redshifts estimated in this way will generally be underestimates, because nine sources lie below the $\pm 1\sigma$ range, while only three sources lie above this range. Fig. 6 shows the difference between the spectroscopic redshift and the redshift estimated from the median curve in Fig. 5. This figure shows that for approximately half the SMSs the method works quite well, leading to redshift errors of $\Delta z < 0.5$. However, there are also a significant number of SMSs where the method results in a catastrophic redshift error. Similar results are obtained if the other sets of low-redshift templates are used. In Table 3 we have listed redshifts estimated in this way for the 14 CUDSS sources with secure identifications.

9.2 Photometric redshifts

A method that has not been used before to estimate the redshifts for SCUBA galaxies is to use multiband optical and IR photometry to estimate photometric redshifts, a method that was first used extensively in the studies of the *Hubble Deep Field*. We are in a good position to examine the utility of this method for SCUBA galaxies, because we have observations in five different photometric bands: U-, B-, V- and I-band photometry from the CFDF and our own K-band photometry. Table 3 lists the multiband photometry for our

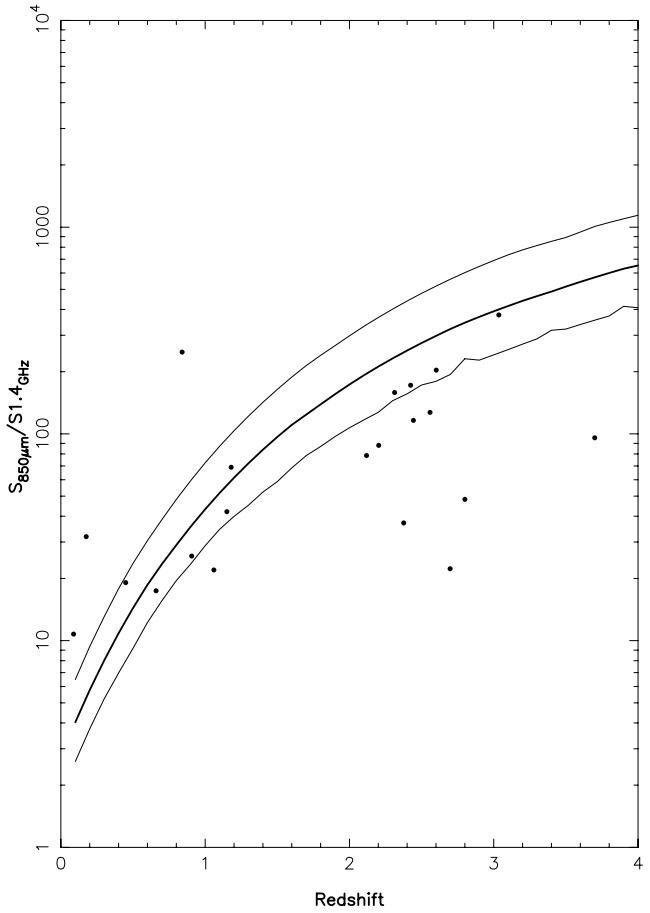

Figure 5. The ratio of 850-μm flux to 1.4-GHz flux verses redshift. The lines show predictions of how this flux ratio should depend on redshift for star-forming galaxies using the method described in Dunne et al. (2000b) and in the text. The middle line shows the median prediction of the templates and the two other lines show $\pm 1\sigma$ predictions based on the range of predicted values at each redshift. The points show SMSs with spectroscopic redshifts and radio detections. The data are from Eales et al. (2000), Smail et al. (2000), Ivison et al. (2002), Chapman et al. (2002, 2003a), Simpson et al. (2004) and this paper.

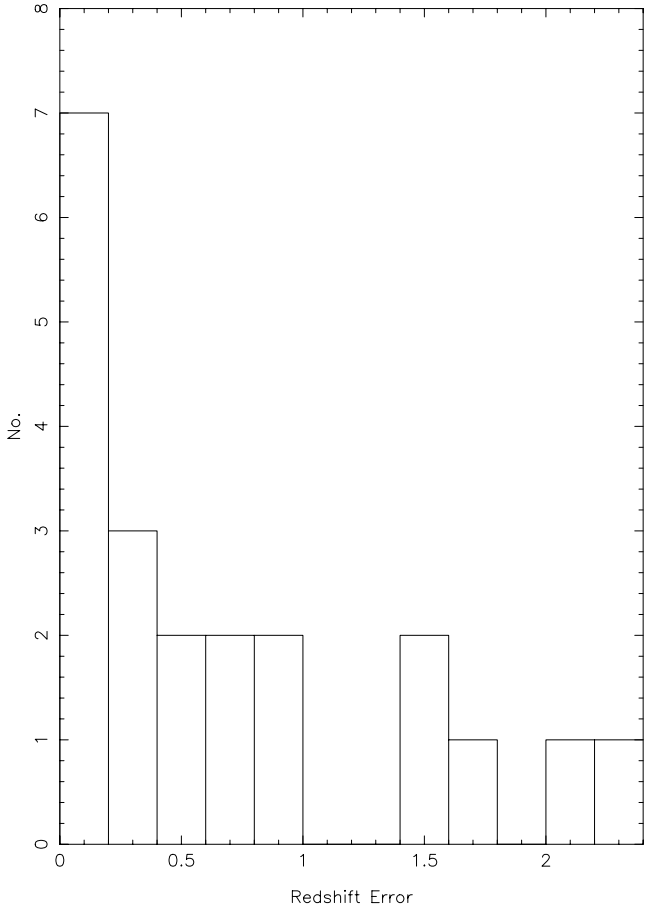

Figure 6. The difference between the spectroscopic redshift and the redshift estimated from the radio method for the 21 SMSs with spectroscopic redshifts and radio measurements. We have estimated the redshift of each SMS using the median prediction in Fig. 5.

14 secure identifications and multiband photometry for two other SCUBA galaxies that have spectroscopic redshifts.

We have used the photometric redshift programme of Benitez (2000). Starting from an ensemble of spectral energy distributions (SEDs) for low-redshift galaxies, the programme determines the redshift and SED that provide the best fit to the multiband photometry of the galaxy in question. The attractive feature of the programme is that it uses Bayes' theorem to incorporate some prior knowledge about the galaxy population, an approach that reduces the number of catastrophic redshift errors. The programme does not incorporate any theoretical assumptions about galaxy evolution and does not allow for the possibility of dust reddening. However, it is impressively successful at matching the spectroscopic redshifts in the Hubble Deep Field (Benitez 2000) and in the Canada–France Redshift Survey (Waskett et al. 2004). Table 3 lists the redshifts estimated using this programme.

SCUBA galaxies, of course, must contain large amounts of dust and thus one might expect any photometric redshift technique to break down when dealing with objects like this. Fig. 7 shows the redshift estimates plotted against the spectroscopic redshifts for the six SCUBA galaxies with both spectroscopic redshifts and enough multiband data to make the photometric technique worth while. The error bars on the photometric redshifts show the redshift range in which there is a probability of 95 per cent that the true redshift lies. For five of the six sources, the agreement between the spectroscopic and photometric redshift is very good and for the remaining source the disagreement is within the range of the errors. Therefore, although this is a small sample, we conclude that estimating the redshifts of SCUBA galaxies from multiband photometry is at least as accurate as estimating the redshifts from the ratio of radio-to-submillimetre flux.

Fig. 8 shows the two sets of redshift estimates plotted against each other. With the exception of CUDSS 3.2, there is surprisingly good agreement between the two sets, suggesting that for the CUDSS sources we can have some confidence in our redshift estimates. We note that many of the estimated redshifts lie in the so-called redshift desert, $1 \leqslant z \leqslant 2$, a range for which there are no bright emission lines in the optical waveband. It may therefore be quite difficult to measure redshifts for some of these galaxies.

The good agreement between the two sets of redshift estimates is the third piece of evidence that gravitational lensing is not generally important (Section 7). If lensing were important, there would be no reason why the estimates should agree, because the photometric-redshift method would yield the redshift of the lens and the radio-to-submillimetre method would yield the redshift of the lensed object.

Table 3. Magnitudes and redshifts.

(1) Name	(2) U_{AB}	(3) B_{AB}	(4) V_{AB}	(5) R_{AB}	(6) I_{AB}	(7) K_{AB}	(8) z_{phot}	(9) z_{spec}	(10) z_{radio}
CUDSS 3.2	23.63 ± 0.05	23.33 ± 0.02	22.63 ± 0.02	...	21.38 ± 0.01	20.55 ± 0.02	0.62 ± 0.21	...	>1.7
CUDSS 3.6	>26.98	>26.38	26.48 ± 0.41	...	>25.62	23.39 ± 0.21	$1.57^{+0.76}_{-0.46}$	...	1.35 ± 0.33
CUDSS 3.7	>26.98	>26.38	>26.40	...	>26.52	22.36 ± 0.09	...	...	2.1 ± 0.6
CUDSS 3.8	20.09 ± 0.01	19.09 ± 0.003	18.25 ± 0.002	...	17.33 ± 0.001	16.47 ± 0.003	0.25 ± 0.16	0.088	0.4 ± 0.18
CUDSS 3.10	21.20 ± 0.01	20.54 ± 0.01	19.07 ± 0.004	...	19.19 ± 0.002	18.22 ± 0.005	0.40 ± 0.18	0.176	0.85 ± 0.23
CUDSS 3.15	24.39 ± 0.07	23.75 ± 0.02	23.31 ± 0.03	...	21.90 ± 0.01	20.24 ± 0.02	0.73 ± 0.23	...	0.6 ± 0.18
CUDSS 3.17	>26.98	>26.38	26.48 ± 0.41	...	>25.62	>22.84	...	...	1.60 ± 0.42
CUDSS 3.24	25.63 ± 0.16	24.85 ± 0.06	24.73 ± 0.08	...	23.22 ± 0.02	21.17 ± 0.07	1.14 ± 0.28	...	1.0 ± 0.25
CUDSS 3.25	25.29 ± 0.14	25.62 ± 0.21	24.72 ± 0.08	...	23.82 ± 0.03	22.47 ± 0.17	$1.05^{+0.27}_{-0.65}$	...	0.4 ± 0.18
CUDSS 14.1	27.17 ± 0.32	26.60 ± 0.12	26.28 ± 0.11	...	24.71 ± 0.04	21.18 ± 0.03	1.25 ± 0.3	...	1.9 ± 0.48
CUDSS 14.3	24.71 ± 0.06	24.55 ± 0.03	24.06 ± 0.02	...	23.19 ± 0.01	21.23 ± 0.04	1.11 ± 0.3	...	1.11 ± 0.3
CUDSS 14.9	>26.98	26.62 ± 0.12	26.40 ± 0.13	...	24.89 ± 0.05	21.12 ± 0.03	1.44 ± 0.32	...	1.7 ± 0.43
CUDSS 14.13	23.93 ± 0.05	23.73 ± 0.02	22.90 ± 0.01	...	20.86 ± 0.004	18.42 ± 0.03	0.90 ± 0.25	1.15	1.2 ± 0.3
CUDSS 14.18	22.97 ± 0.03	22.57 ± 0.01	21.99 ± 0.01	...	20.61 ± 0.003	18.95 ± 0.01	0.69 ± 0.22	0.66	0.7 ± 0.2
N2 850.4[a]	...	...	22.40 ± 0.03	22.47 ± 0.01	22.45 ± 0.02	18.43 ± 0.02	$1.3^{+1.18}_{-0.3}$	2.376	...
N2 850.8[a]	...	...	22.79 ± 0.03	22.68 ± 0.02	22.17 ± 0.02	20.06 ± 0.09	1.41 ± 0.32	1.189	...

(1) Source name. (2)–(7) Magnitudes in the AB system in the different photometric bands. Except where noted, the optical magnitudes are from the CFDF Survey (Section 3) and the IR magnitudes are from this paper. In both cases, the errors on the magnitudes do not include the calibration error, which is approximately 0.05 mag. (8) Redshift estimated using the photometric redshift method of Benitez (2000). (9) Spectroscopic redshift. (10) Redshift estimated from the ratio of radio-to-submillimetre flux. Notes on sources: [a]the data for these objects were taken from Ivison et al. (2002).

10 DISCUSSION

In this section we will discuss what the optical, IR and radio observations of the CUDSS sources reveal about the nature of SMSs. A later paper will describe an investigation of the evolution of the submillimetre luminosity function, which will incorporate the new results.

A simple thing we can do is compare the far-IR–submillimetre luminosities of the CUDSS sources with the luminosities of dust sources in the local Universe. A problem that is often skated over in calculating the luminosity of SMSs is that there is usually a flux measurement at only a single wavelength and therefore the calculation of the luminosity requires some assumption about the SED of the SMS. To investigate the effect of this assumption, we have calculated the luminosity of the CUDSS sources making two different assumptions about the SED. We used two extreme SEDs from the sample of *IRAS* galaxies of Dunne et al. (2000a). NGC 958 is a galaxy whose SED is dominated by cold dust. The observed fluxes of this galaxy are fitted well by the two-component dust model of Dunne & Eales (2001), with dust at 20 and 44 K in the ratio by mass of 186:1. At the other extreme is the galaxy IR1525+36, which, in the Dunne & Eales (2001) model, has dust at 19 and 45 K in the ratio by mass of 15:1. Fig. 9 shows the luminosities of the CUDSS sources with secure identifications calculated using these two different assumptions. We have also plotted in Fig. 9 the luminosities of the *IRAS* galaxies in the sample of Dunne et al. (2000a). For the CUDSS galaxies without spectroscopic redshifts, we have used the redshift estimated from our multiband photometry (Section 9.2) and, if that is not possible, the redshift estimated from the ratio of radio-to-submillimetre flux (Section 9.1). The figure shows that there is roughly a difference of a factor of 5 in the luminosities of the CUDSS sources calculated with the two different SEDs, showing the sensitivity of the calculation to the assumption about the SED. With the cold SED, there is a substantial overlap in the luminosities of the CUDSS sources with the low-redshift sample, although the majority of the CUDSS sources are still more luminous than the most luminous object in the local sample, the archetypical ultraluminous infrared galaxy Arp 220.

Given our extensive multiband optical/IR photometry, we can calculate the ratio of dust luminosity to optical/IR luminosity. For each source with a secure identification, we calculated the optical/IR flux by integrating the observed SED from 0.25 to 2.5 μm. We estimated the flux at each wavelength by making a power-law interpolation between the two neighbouring photometric measurements. The biggest uncertainty in this calculation is the question of which SED to use to calculate the dust luminosity. Fig. 10 shows the histogram of dust luminosity divided by optical/IR luminosity, with the dust luminosity calculated using the cold SED. The figure shows that most of the CUDSS sources have dust luminosities that are between 10 and 100 times greater than emission in the optical/near-IR bands. If the hot SED is used to calculate the dust luminosities, these figures increase by a factor of approximately five. Whichever SED is used, Figs 9 and 10 show, as one would expect, that the CUDSS sources are luminous systems with most of the emission being reprocessed emission from dust.

We now compare the absolute magnitudes of the SMSs with those of other high-redshift objects. Dunlop (2002) plotted the K magnitudes of SMSs against their redshifts and compared this diagram to the same diagram for radio galaxies, which are among the most luminous galaxies known. By comparing the apparent magnitudes of SMSs and radio galaxies at the same redshift, he was able to compare the absolute magnitudes of the two types of object. He concluded that the host galaxies of SMSs have absolute magnitudes that are very similar to those of radio galaxies. At redshifts <3, the K-band falls on the long-wavelength side of the 4000-Å break and thus the K-band light is not dominated by the light from young stars, but rather by the light from the stars that form most of the stellar mass of a galaxy. Therefore, one inference that one might draw from the result of Dunlop (2002) is that the host galaxies of SMSs are giant galaxies in which a large fraction of the stars have already formed.

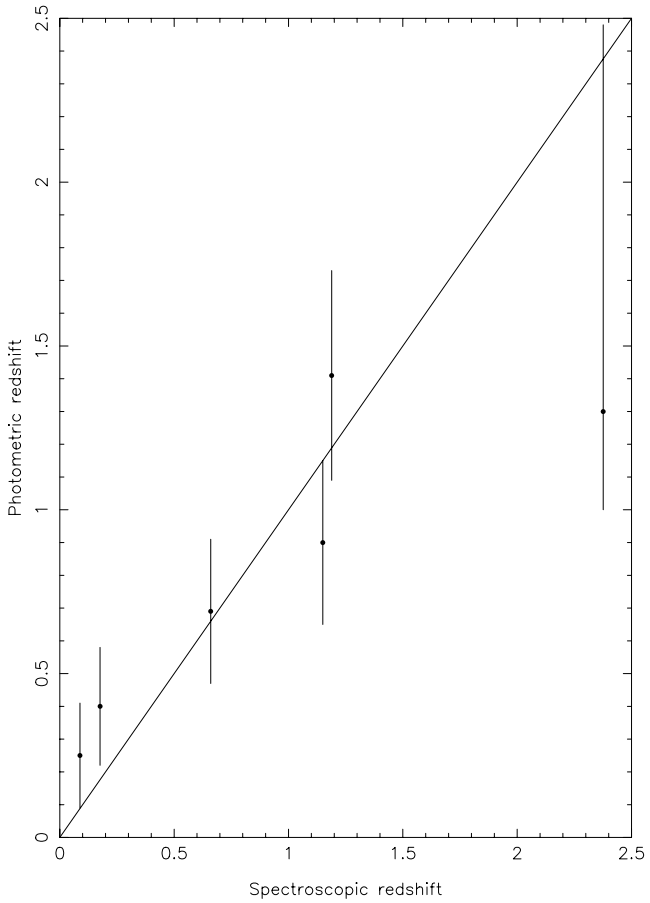

Figure 7. Spectroscopic redshift verses photometric redshift for the six galaxies with extensive multiband photometry and spectroscopic redshifts. The spectroscopic redshift is equal to the photometric redshift along the line.

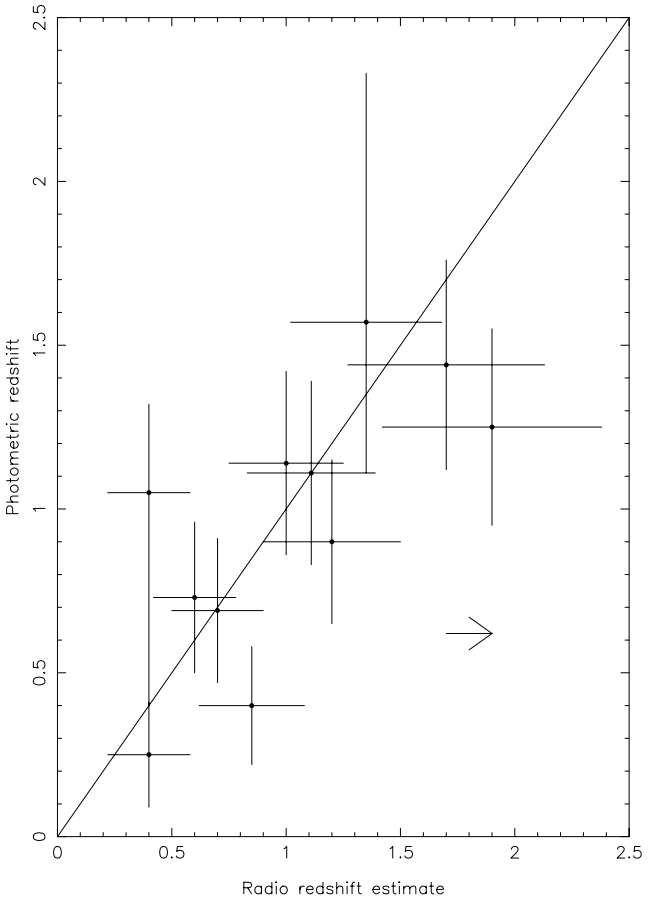

Figure 8. Redshift estimated from the multiband optical and IR photometry verses redshift estimated from the radio-to-submillimetre flux ratio. The arrow is CUDSS 3.2, which has an upper limit for its radio flux.

A limitation of this study, however, was that at that time there were only three SMSs with spectroscopic redshifts. These were also SMSs that were known to be gravitationally lensed, and although Dunlop corrected for this, there is necessarily some uncertainty in the value of the gravitational amplification factor. Because there are now a significant number of SMSs with spectroscopic redshifts, we can now carry out a much more extensive comparison of the magnitudes of SMSs with the magnitudes of other high-redshift objects.

Fig. 11 shows K magnitude plotted against redshift for (a) all SMSs with spectroscopic redshifts that are not known to be lensed and (b) all CUDSS sources with secure identifications. For the CUDSS galaxies without spectroscopic redshifts, we have used the redshift estimated from our multiband photometry (Section 9.2) and, if that is not possible, the redshift estimated from the ratio of radio-to-submillimetre flux (Section 9.1). We have also plotted on the diagram the data for radio galaxies described in Eales et al. (1997). In order to ensure that there are no spurious differences caused by magnitudes being measured in apertures of different sizes, we have corrected all the magnitudes to a common metric aperture. Most of the magnitudes for the SCUBA galaxies have been measured through a 3-arcsec aperture, which at $z = 2$ is equivalent, with our cosmological assumptions (Section 1), to a physical distance of 23.5 kpc. We have converted the photometry for the radio galaxies to this metric aperture using the method described in Eales et al. (1997). The figure confirms the conclusion of Dunlop (2002) that many SMSs have host galaxies that are as luminous as radio galaxies. Approximately half the SMSs are, however, in host galaxies that are fainter than radio galaxies, although the difference is usually small enough that they must still be fairly luminous systems.

Another interesting population with which to compare the SMSs are the galaxies found in μJy radio surveys. The morphologies of these radio sources (Muxlow et al., in preparation) suggest the emission is generally from a star-forming disc rather than being the result of an active nucleus, as is the case for the classical radio galaxies plotted in Fig. 11. Chapman et al. (2003b, and references therein) have carried out a multiwavelength study of these sources. A significant fraction of them are also detected in the submillimetre waveband and Chapman et al. (2003b) argue that there is a substantial overlap between the μJy population and the SMSs. They have also found the interesting result that the optical absolute magnitudes of the μJy radio sources have a small range, with most of the host galaxies having an optical luminosity fairly close to L_*. They speculate that the reason for this may be that less luminous, and therefore less massive, galaxies are less efficient at confining cosmic rays.

We have taken the median I-band absolute magnitude and $I - K$ colour given in Chapman et al. (2003b) to estimate the median K-band absolute magnitude, which we have then used to predict a K–z relationship for these objects. This is shown in Fig 11. It passes neatly through the middle of the SMS points, which suggests that the host galaxies of SMSs and μJy radio sources are very similar in their optical/IR luminosities. The colours of the two classes are also

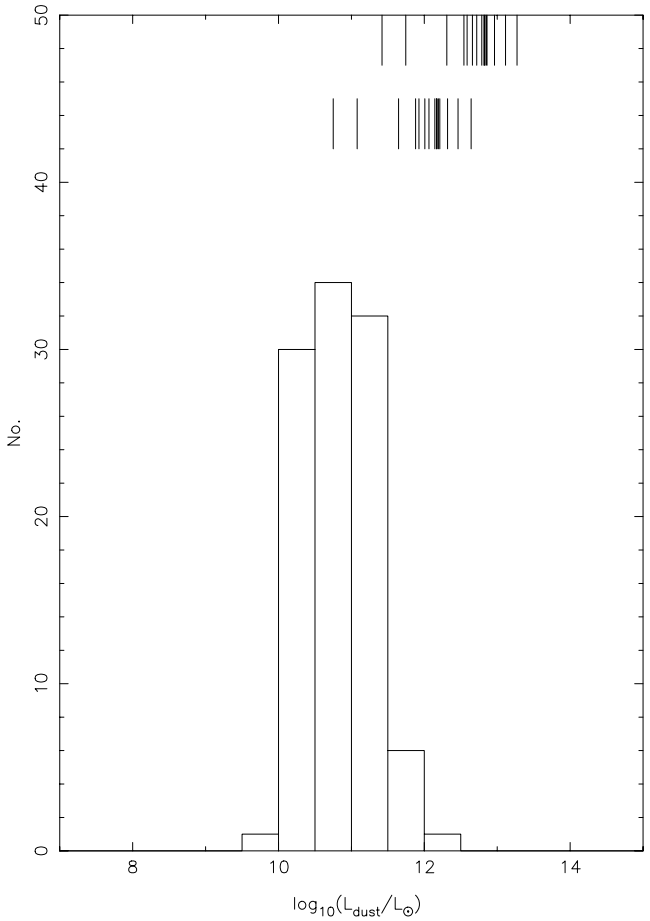

Figure 9. The far-IR–submillimetre luminosities of the CUDSS sources with secure identifications and of the *IRAS* galaxies in the sample of Dunne et al. (2000a). The histogram shows the luminosities of the *IRAS* galaxies. The lower set of vertical lines mark the luminosities of the CUDSS sources calculated using the SED of NGC 958 (see text); the upper set of lines show the luminosities calculated using the SED of IR1525+36.

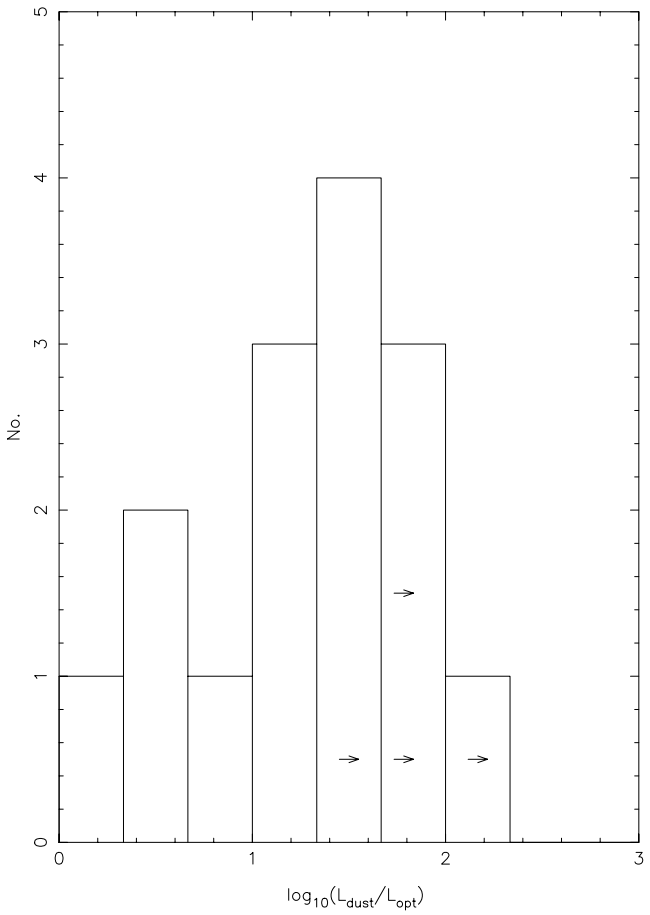

Figure 10. Histogram of the ratio of dust luminosity to optical/IR luminosity for the CUDSS sources with secure identifications. We have calculated the dust luminosity using the SED of NGC 958 (see text). The lower limits are for sources that have not yet been detected in the optical/IR.

quite similar. The median $I - K$ colour of the CUDSS sources with secure identifications is 3.3, very similar to the value of 3.4 given by Chapman et al. (2003b) for the optically-faint μJy radio sources. Therefore, both the colours and the optical/IR luminosities of the host galaxies are additional pieces of evidence that there is, at the least, a substantial overlap between the two populations.

It might be thought that the identification of SMSs with luminous galaxies is an argument against these objects being at an early stage of galactic evolution, because a large number of stars have clearly already formed. This is not necessarily so. Simple models of the evolution of dust in a galaxy (Dunne et al. 2003, and references therein) imply that the mass of dust in a galaxy will be at a maximum when roughly half the stars are formed. With the caveat that the submillimetre luminosity also depends on dust temperature, the time when the dust mass is at its greatest will also be the time at which the submillimete luminosity is at its peak. How close this time is to the time at which star formation started in the galaxy depends on the characteristic time-scale of star formation. If most of the stars form in a burst, as may well be the case for elliptical galaxies, the interval between the onset of star formation and the time when half the stars have formed may be very short indeed. If these ideas are correct, then the SMSs plotted in the figure will be roughly a factor of two more luminous in the optical/near-IR waveband by the current epoch.

11 CONCLUSIONS

We have presented optical, near-IR and radio observations of the 3-hour field of the CUDSS. We have reached the following conclusions.

(i) Of the 27 submillimetre sources in this field, nine have secure identifications with either a radio source or a near-IR source. Of the 50 submillimetre sources in the two CUDSS fields, 14 now have secure identifications.

(ii) The percentage of sources with secure identifications is consistent with that found for the bright 8-mJy submillimetre survey, once allowance is made for the different submillimetre and radio flux limits.

(iii) Of the 14 secure identifications, eight are VROs or EROs, five have colours typical of normal galaxies, and one is a radio source that has not yet been detected at optical/IR wavelengths. These proportions are very similar to those found for the 8-mJy survey. Eleven of the identifications have optical/near-IR structures which are either disturbed or have some peculiarity that suggests that the host galaxy is part of an interacting system, a similar percentage to that found for the 8-mJy survey.

(iv) We have examined the reliability of the CUDSS catalogue. In contrast to the result of a similar analysis for the 8-mJy survey, we find no clear evidence that CUDSS sources with a low

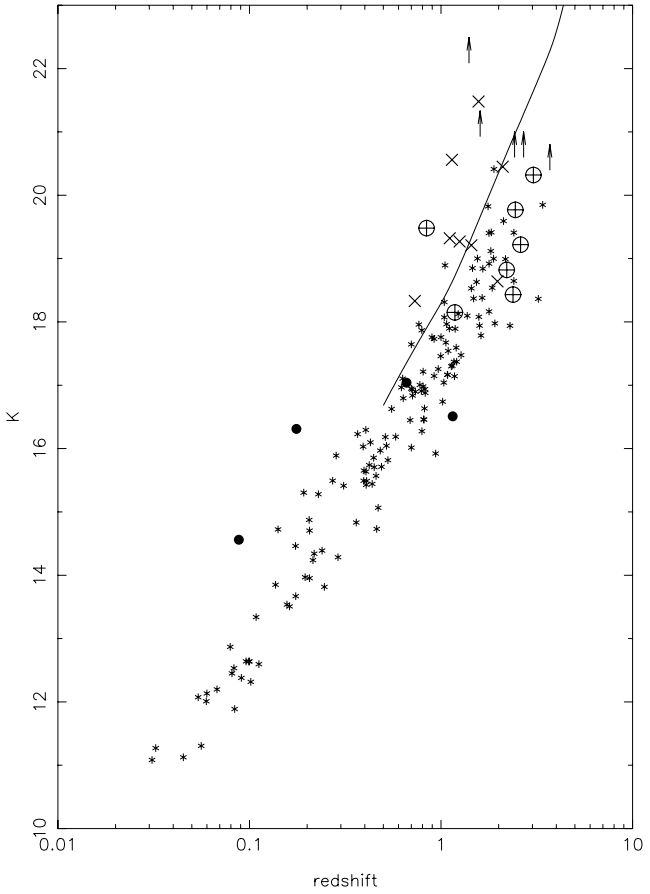

Figure 11. *K*-band magnitude verses redshift for SCUBA galaxies and radio galaxies. The stars show the positions of the samples of radio galaxies described in Eales et al. (1997). The other symbols represent SMSs. The filled circles are for CUDSS sources with secure identifications and spectroscopic redshifts. The crosses-in-circles show other SMSs with spectroscopic redshifts (Chapman et al. 2003a). The crosses represent CUDSS sources with secure identification but only estimated redshifts (see text). The lower limits are for SMSs with secure identifications with radio sources but which are undetected in the *K* band. Three of these have spectroscopic redshifts (Chapman et al. 2003a) and two are CUDSS sources for which we have estimated redshifts from the ratio of radio-to-submillimetre flux. The line shows the predicted relation for μJy radio sources (see text).

signal-to-noise ratio or at positions in the submillimetre maps where the noise is high are any less reliable than the rest of the sources.

(v) We have critically examined different methods of estimating the redshifts of SMSs. We show that the method of estimating redshifts from the ratio of radio-to-submillimetre flux (Carilli & Yun 1999) works well for approximately 50 per cent of SMSs, but there are a significant number of catastrophic errors. We show the method of estimating redshifts from the multiband optical and near-IR photometry works surprisingly well.

(vi) We conclude that the low-redshift identifications are genuine low-redshift submillimetre sources rather than being gravitational lenses. This conclusion is based on (1) the morphologies of the identifications, (3) the good agreement between the photometric redshifts of the galaxies and the redshifts estimated from the ratio of radio-to-submillimetre flux, (3) the fact that the majority of the low-redshift identifications are also 15-μm sources.

(vii) We show that many SMSs are in host galaxies that are as bright in the near-IR as radio galaxies, which are among the most luminous galaxies in the Universe. However, on average, the host galaxies of SMSs are slightly less bright in the near-IR than the classical radio galaxies. They are, however, very similar, in both their absolute near-IR/optical magnitudes and colours, to the host galaxies of the radio sources detected in μJy radio surveys.

ACKNOWLEDGMENTS

Research by DC, SE, RI and WG is supported by the Particle Physics and Astronomy Research Council. SE thanks the Leverhulme Trust for the award of a research fellowship during a critical phase in this research. LD is supported by a PPARC fellowship and KW by a PPARC studentship.

REFERENCES

Alexander D. M. et al., 2003, AJ, 125, 383
Almaini O. et al., 2003, MNRAS, 338, 303
Appleton P. N., Marston A. P., 1997, AJ, 113, 201
Barger A. J., Cowie L. L., Sanders D. B., Fulton E., Taniguchi Y., Sato Y., Kawara K., Okuda H., 1998, Nat, 394, 428
Benitez N., 2000, ApJ, 536, 571
Bertoldi F. et al., 2000, A&A, 360, 92
Bertoldi F., Menten K. M., Kreysa E., Carilli C. L., Owen F., 2001, in Rickman H., ed., Proc. XXIV IAU General Assembly, Highlights of Astronomy, Vol. 12. Astron. Soc. Pac., San Francisco, p. 473
Blain A. W., 1998, MNRAS, 297, 502
Blain A. W., Kneib J.-P., Ivison R. J., Smail I., 1999, MNRAS, 512, 87
Brinchmann J. et al., 1998, ApJ, 499, 112
Carilli C. L., Yun M. S., 1999, ApJ, 513, L13
Carilli C. L., Yun M. S., 2000, ApJ, 530, 618
Chapman S. C., Smail I., Ivison R. J., Blain A. W., 2002, MNRAS, 335, L17
Chapman S. C., Blain A. W., Ivison R. J., Smail I. R., 2003a, Nat, 422, 695
Chapman S. C. et al., 2003b, ApJ, 585, 57
Cole S., Lacey C. G., Baugh C. M., Frenk C. S., 2000, MNRAS, 319, 168
Cowie L. L., Gardner J. P., Hu E. M., Songaila A., Hodapp K.-W., Wainscoat R. J., 1994, ApJ, 434, 114
Downes A. J. B., Peacock J. A., Savage A., Carrie D. R., 1986, MNRAS, 218, 31
Dunlop J. S., 2002, in Shanks T., Metcalfe N., eds, ASP Conf. Ser. Vol. 283, A New Era in Cosmology. Astron. Soc. Pac., San Francisco, p. 381
Dunne L., Eales S., Edmunds M., Ivison R., Alexander P., Clements D., 2000a, MNRAS, 315, 115
Dunne L., Clements D., Eales S., 2000b, MNRAS, 319, 813
Dunne L., Eales S., 2001, MNRAS, 327, 697
Dunne L., Eales S., Edmunds M., 2003, MNRAS, 341, 589
Eales S. A., Rawlings S., Law-Green D., Cotter G., Lacy M., 1997, MNRAS, 291, 593
Eales S. A., Lilly S., Gear W., Dunne, L., Bond J. R., Hammer F., Le Fèvre O., Crampton D., 1999, ApJ, 515, 518
Eales S. A., Lilly S., Webb T., Dunne L., Gear W., Clements D., Yun M., 2000, AJ, 120, 2244
Eggen O., Lynden-Bell D., Sandage A., 1962, ApJ, 136, 748
Flores H. et al., 1999, ApJ, 517, 148
Gear W. K., Lilly S. J., Stevens J. A., Clements D. L., Webb T. M., Eales S. A., Dunne L., 2000, MNRAS, 316, L51
Hammer F., Crampton D., Le Fèvre O., Lilly S. J., 1995, ApJ, 455, 88
Hogg D. W., 2001, AJ, 121, 1207
Hughes D. H. et al., 1998, Nat, 394, 241
Ivison R., Smail I., Barger A. J., Kneib J.-P., Blain A. W., Owen F. N., Kerr T. H., Cowie L. L., 2000, MNRAS, 315, 209
Ivison R. J. et al., 2002, MNRAS, 337, 11
Larson R. B., 1975, MNRAS, 173, 671

Lilly S. J., Le Fèvre O., Crampton D., Hammer F., Tresse L., 1995, ApJ, 455, 50
Lilly S., Eales S., Gear W., Hammer, F., Le Fèvre O., Crampton D., Bond J. R., Dunne L., 1999, ApJ, 518, 641
McCracken H. J., Le Fèvre O., Brodwin M., Foucaud S., Lilly S. J., Crampton D., Mellier Y., 2001, A&A, 376, 756
Percival W. J., Scott D., Peacock J. A., Dunlop J., 2003, MNRAS, 338, L31
Rengarajan T. N., Takeuchi T., 2001, PASJ, 53, 433
Richards E. A., 2000, ApJ, 533, 611
Scott S. et al., 2002, MNRAS, 331, 817
Serjeant S. et al., 2003, MNRAS, 344, 887
Simpson C., Dunlop J. S., Eales S. A., Ivison R. J., Scott S. E., Lilly S. J., Webb T. M. A., 2004, MNRAS, submitted
Smail I., Ivison R. J., Blain A. W., 1997, ApJ, 490, L5
Smail I., Ivison R. J., Owen F. N., Blain A. W., Kneib J.-P., 2000, ApJ, 528, 612
Smail I., Owen F. N., Morrison G. E., Keel W. C., Ivison R. J., Ledlow M. J., 2002, ApJ, 581, 844
Smail I., Chapman S. C., Ivison R. J., Blain A. W., Takata T., Heckman T. M., Dunlop J. S., Sekiguchi K., 2003, MNRAS, 342, 1185
Sutherland W., Saunders W., 1990, MNRAS, 259, 413
Waskett T. et al., 2003, MNRAS, 341, 1217
Waskett T., Eales S. A., Gear W. K., McCracken H. J., Brodwin M., Nandra K., Laird E. S., Lilly S., 2004, MNRAS, 350, 785
Webb T. et al., 2003a, ApJ, 582, 6
Webb T., Eales S., Lilly S. J., Clements D. L., Dunne L., Gear W. K., Flores H., Yun M., 2003b, ApJ, 587, 41 (W2003)
Webb T., Lilly S. J., Clements D. L., Eales S. A., Yun M., Brodwin M., Dunne L., Gear W. K., 2003c, ApJ, 597, 680

This paper has been typeset from a TEX/LATEX file prepared by the author.